AD NUMBER

AD906784

LIMITATION CHANGES

TO:

Approved for public release; distribution is unlimited.

FROM:

Distribution authorized to U.S. Gov't. agencies only; Test and Evaluation; 29 JAN 1973. Other requests shall be referred to Naval Ordnance Laboratory, Attn: Code 212, Silver Spring, MD 20910.

AUTHORITY

USNCL ltr, 29 Aug 1974

Naval Ordnance Laboratory

Annual Progress Report for the Period

1 June 1971 through 30 May 1972

ARPA Order 1597

EPITAXIAL SUBLIMATION METHODS FOR THE STUDY OF PSEUDO-BINARY SEMICONDUCTOR ALLOYS

INTRODUCTION

This annual report describes work performed under ARPA Order 1597 at the Naval Ordnance Laboratory. This portion of the ARPA program centers on surface properties affecting the electro-optical behavior of semiconductors particularly the IV-VI semiconductors and alloys used in infrared emitters and detectors. These surface properties are dominated by chemisorbed impurities. (Related effects produced by electromigration of impurity ions dominate the electrical properties of the semiconductor-oxide interface.) In IV-VI device technology chemisorption effects are both strong and diverse, determining carrier populations in surface regions and throughout film structures, producing sensitization and aging, and, as we have now shown, affecting the quality of epitaxial growth.

The primary purpose of the NOL ultra-high vacuum experimental effort is to clarify the nature of the interaction of gases, primarily O_2 and H, with epitaxial IV-VI films. Previous studies[1-6] of the effects of chemisorption on the electrical properties of IV-VI films have been carried out in relatively

modest vacua and/or on films that had been exposed to the atmosphere. As a consequence, the role of contamination in these experiments is unknown, and the results ambiguous. In the NOL program, adsorption studies are made on films which have been grown and maintained under ultra-high vacuum conditions. The Hall and resistivity measurements are made in situ, and ambiguities due to contamination eliminated. Thus far, we have obtained a number of significant new results bearing on a) film growth; b) hydrogen adsorption on PbS; and c) the oxidation of PbS. In addition, we have formulated a new method of analyzing transport data which substantially reduces the difficulty of interpreting the behavior of two-carrier films. Details of this work and its implication for IV-VI thin film device technology are given in sections 1, 2, 3, and 4.

The chemical state of contaminated IV-VI surfaces is responsible for many of the most important electro-optical properties, but is not explained well by bulk chemistry. Many special methods of experimental surface analysis have been devised for determining the chemical species present and their bond structure. We have built the simplest of such surface analysis tools, an appearance potential spectroscopy (APS) apparatus. APS uses an electron beam to probe the core states of surface atoms, measuring the threshold of X-ray florescence core de-excitation. The spectrometer has been assembled and the electronics is being tested. Details are given in Section 5.

Our theoretical studies have made important advances in the understanding of the effect of chemisorption on the electrical properties of semiconductors. We have completed[16] a detailed calculation of carrier scattering by charged chemisorbed ions. This takes into account for the first time the actual three dimensional screened space charge potential of the surface charge array, the interference terms between electrons scattered from different surface charges, and the dielectric image force; all these effects are shown to be quite important. These results are now being used as the basis of a realistic surface transport theory to predict surface mobility, surface Hall coefficient, and surface magnetoresistance. We have also made a breakthrough in the theory of semiconductor surfaces with the discovery[17,18] of a new and basic theoretical relation between surface scattering rates and chemisorption thermodynamics. This new relation is based on the structure factor of the array of chemisorption charges on the surface. We are following this up with calculations of the adsorption isotherms of various gases on semiconductor surfaces. Progress has also been made on the quantum theory of the dispersive dielectric image force, which we have shown to be important in surface mobility, etc., and which is well-known to strongly affect surface recombination rates, heterojunction tunneling etc. Details of this work are given in sections 6, 7, 8, 9, and 10.

RESEARCH PROGRESS

1. Film Growth (Experimental: R. N. Lee)

We find that the room temperature mobilities in our ultra-high vacuum grown PbS films are comparable to or better than those in the best films grown in less elaborate vacuum systems. The measured room temperature mobilities range from approximately 500 cm^2/volt-sec. to as high as 750 cm^2/volt-sec. The higher values approach the highest mobilities that have been observed in bulk material.

We have considered the possibility that the high apparent mobilities are due to the formation of a surface layer of lead. The growth of such layers has been reported for sublimated PbS films,[7] and would lead to an anomalously high apparent mobility for the PbS. The measured mobility for such a film would be the resultant of the carrier mobility in the lead layer and the mobility in the underlying PbS layer. This possibility may be rejected, however, on the basis of the adsorption results to be discussed later in this report. The adsorption data clearly indicate that there is only one carrier type (i.e. only one mobility) in the film, and we may have confidence in the high measured values of the mobilities.

The superior quality of the ultra-high vacuum grown films gives us significant new insight into the mechanisms of growth and strain relief on NaCl substrates. Epitaxial IV-VI films are commonly grown in vacua of $\sim 10^{-5}$ Torr with water vapor comprising 90% or more of the background gas. A popular conjecture has been that the water is necessary for good film growth in that it allows the NaCl to flow plastically and/or provides a buffer between the substrate and the film. This

idea must now be discarded, for the water vapor in the ultra-high vacuum system is completely negligible and the substrates were thoroughly degassed prior to deposition of the films.

These results suggest that substantial improvements in device quality could be obtained through the use of ultra-high vacuum during device fabrication. We note, in fact, that bakeout of the vacuum system was one of the procedures employed by Holloway et al[3] in obtaining their very high mobility films, and we suggest that this procedure is of greater importance than has previously been appreciated.

2. Adsorption of Atomic Hydrogen (Experimental: R. N. Lee)

One of the major results of recent work by Zemel and co-workers[4,5] at the University of Pennsylvania has been that the electrical properties of epitaxial lead chalcogenide films are highly sensitive to atomic hydrogen. The hydrogen effects observed were completely reversible, and Zemel has suggested[9] that hydrogen adsorption may provide a non-destructive measure of the lead vacancy concentration in lead salt films. This exciting possibility presupposes a model in which the hydrogen occupies lead vacancy sites.[4,5] The circumstances of the previous studies were such, however, that the hydrogen effect could be associated with the presence of oxygen on the film rather than with the lead vacancies, and it is of some importance to examine the interaction of hydrogen with the lead salts in the absence of oxygen contamination. For this reason, we have studied the adsorption of hydrogen on ultra-high vacuum grown PbS films. The adsorption effects were observed by means of in situ measurements of the Hall coefficient and the resistivity.

The ultra-high vacuum studies have verified the major features of hydrogen adsorption which were previously reported. That is, molecular hydrogen has no observable effect on the electrical properties; whereas atomic hydrogen adsorbs reversibly to produce relatively large changes in the carrier population. Atomic hydrogen acts as a donor, and it is incorporated into the film without producing significant changes in the electron mobility.

Figure 1 is an R_H versus ρ plot which resulted from exposure to atomic hydrogen. This data is somewhat complicated, and the lettered key points in the plot are identified in Table 1. The major points to be derived from this plot are that the hydrogen increased the electron population by up to 6.5×10^{12} cm^{-2} and that the data points fell along a constant mobility line as long as the temperature variation remained negligible.

In our investigations, the atomic hydrogen was generated by a beam of 70 eV electrons in the ionization stage of the residual gas analyzer mounted on the experimental chamber, and the atomic hydrogen so produced had to make several collisions with the chamber walls before reaching the sample. The effective partial pressure of atomic hydrogen at the sample is thus very difficult to estimate. It was assumed, however, that the amount of atomic hydrogen at the sample was proportional to the total hydrogen pressure in the system as measured by a Bayard-Alpert gauge. It should be pointed out that the metal walls in the baked ultra-high vacuum system pump atomic hydrogen much more efficiently than the

TABLE I

KEY TO FIGURE 1

Key Letter	Event
a	The residual gas analyzer was turned on, resulting in an increased pressure and production of atomic hydrogen at a pressure estimated to be no higher than 5×10^{-10} Torr.
b	After six hours, the RGA was turned off.
c	Hydrogen gas was admitted to the experimental chamber at a pressure of 5×10^{-3} Torr.
d	A baffled ionization gauge was turned on, producing a small amount of atomic hydrogen at the sample.
e	The RGA ionizer was turned on to generate atomic hydrogen more efficiently.
f	This extreme data point was taken immediately after turning on the RGA. Data points taken during the subsequent decrease in pressure fell along f-g.
g	The total hydrogen pressure was stabilized at 5×10^{-5} Torr.
h	The pressure was again allowed to fall, and data points along h-k were taken.
k	The pressure was again raised to the 10^{-5} Torr range. Subsequent variations in pressure and temperature resulted in the data points lying between e-g and h-k.

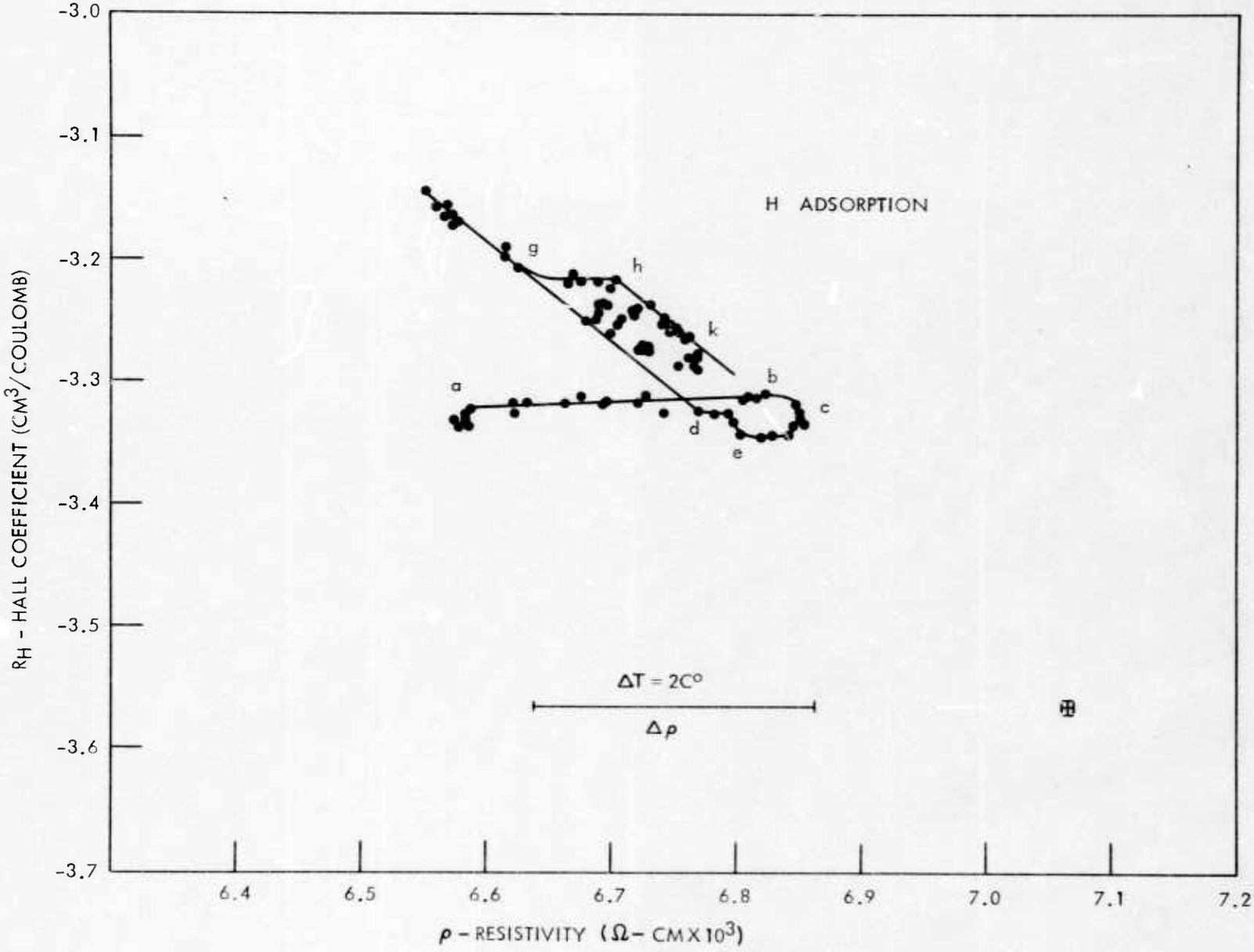
H ADSORPTION
-3.0
-3.1
-3.2
-3.3
-3.4
-3.5
-3.6
-3.7
R_H - HALL COEFFICIENT (CM^3/COULOMB)
6.4
6.5
6.6
6.7
6.8
6.9
7.0
7.1
7.2
ρ - RESISTIVITY (Ω - CM X 10^3)
a
b
c
d
e
g
h
k
ΔT = 2C°
Δρ

FIG. 1

unbaked glass walls of the chambers used in the previous studies, and the effective pressure of atomic hydrogen was undoubtedly much lower. This difference in pressure regimes is reflected in the data.

The lower atomic hydrogen pressures used in the present study resulted in the observation of some previously unreported aspects of the adsorption. We have found that the hydrogen uptake at these pressures is a function of pressure over a pressure range of more than four orders of magnitude. That is, when a constant hydrogen pressure was established, the electron population quickly stabilized at a steady-state value which depended on the pressure. A plot of the steady state electron population versus total hydrogen pressure is presented in Fig. 2.

The kinetics of the hydrogen adsorption could not readily be determined in the ultra-high vacuum studies due to the well-known 'pump-down' effect. As soon as the electron beam was turned on, the pumping of the atomic hydrogen produced caused a rapid drop in the total pressure, and it was usually many minutes before a steady state was achieved. During this time, the effective pressure of atomic hydrogen at the sample was not proportional to the total hydrogen pressure and it certainly was not constant.

When the hydrogen pressure was suddenly changed from one constant value to another, the new steady-state value of the electron population was usually established more quickly than could be followed with our point-by-point measurement technique.

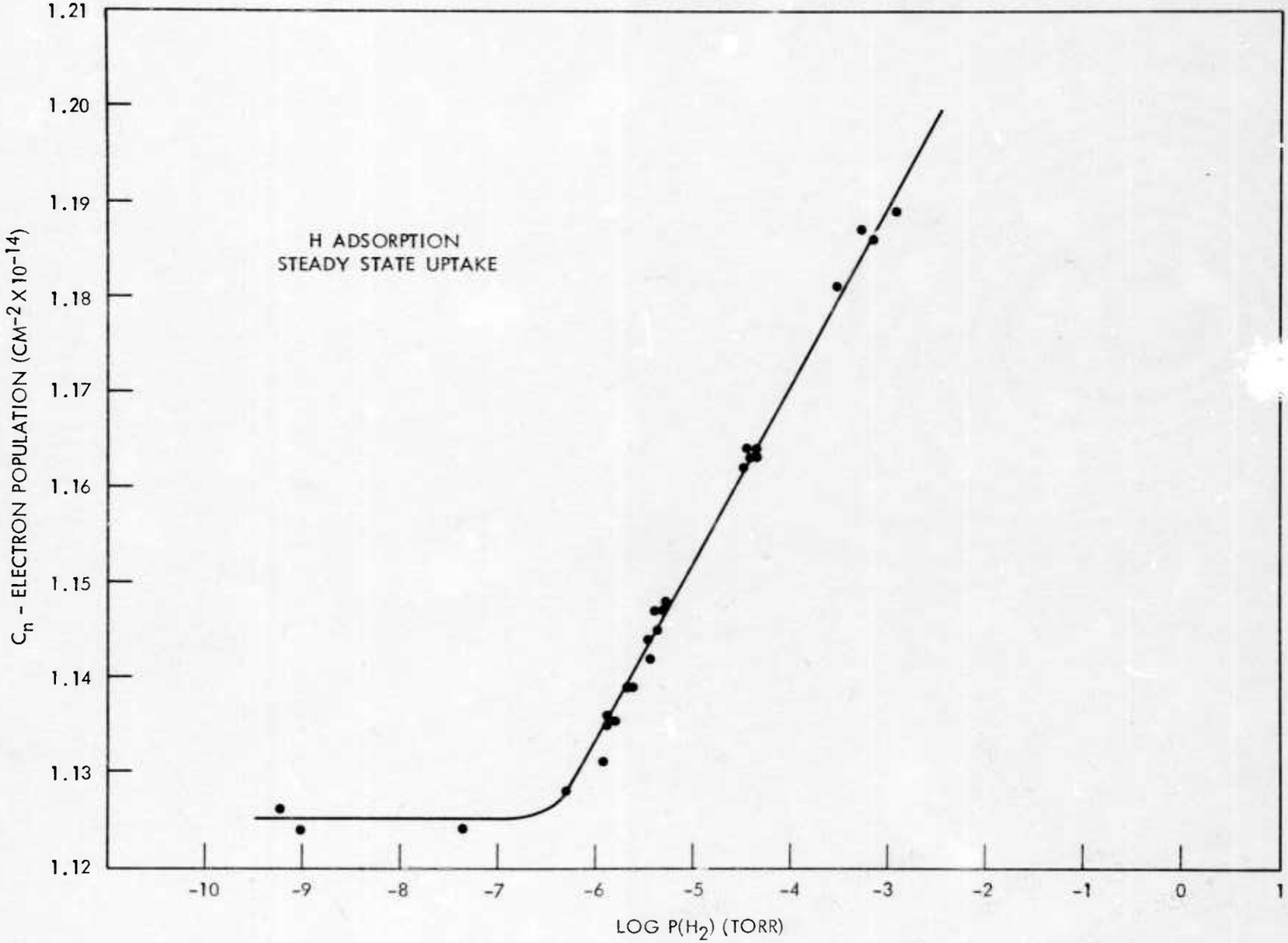
H ADSORPTION
STEADY STATE UPTAKE
C_n - ELECTRON POPULATION ($CM^{-2} \times 10^{-14}$)
1.21
1.20
1.19
1.18
1.17
1.16
1.15
1.14
1.13
1.12
-10
-9
-8
-7
-6
-5
-4
-3
-2
-1
0
1
LOG $P(H_2)$ (TORR)

FIG. 2

We are now changing our instrumentation to provide a continuous recording of both the resistivity and Hall voltages, however, and the kinetics of these transitions should be available in the future.

The adsorption data have all been plagued with the effects of temperature drifts. Although the effects are quite large, no mention of these difficulties has been made in recent reports of similar transport studies. The problem arises as a consequence of the $T^{-5/2}$ temperature dependence of the mobility in the lead salts. This temperature dependence implies that a 1 C° temperature change at room temperature produces a 0.8% change in the resistivity, and this result is entirely consistent with our observations. Normal short term temperature variations in our laboratory are of the order of a degree, and a five degree drift over a four hour period is not unusual. These temperature fluctuations correlate well with the scatter of the resistivity data, and are primarily responsible for the relatively large scatter in the data of Fig. 1. The horizontal bar in the lower part of this figure indicates the resistivity change predicted by the $T^{-5/2}$ dependence for a two degree temperature drift. The oxygen adsorption data which are discussed later in this report were obtained during periods when the ambient temperature was relatively stable, and the scatter of these data is significantly smaller.

3. Oxygen Adsorption (Experimental: R. N. Lee)

Our studies of the chemisorption of oxygen on PbS constitute the first examination of the oxidation of a lead chalcogenide to be carried out by means of transport measurements in the very low pressure range. We have made controlled oxygen exposures at pressures ranging from 10^{-8} Torr up to 10^{-2} Torr with partial pressures of background gases less than 10^{-10} Torr. Previous studies[1-6] were carried out with background pressures of 10^{-6} Torr or higher and with oxygen exposures primarily provided by exposing the films to atmosphere. Our results include a number of previously unobserved features of the oxidation of lead chalcogenides and show that some apparent discrepancies between previous studies are the result of differing vacuum conditions.

The effects of exposing PbS to oxygen at pressures up to 10^{-2} Torr are shown in the Hall coefficient versus resistivity plot of Fig. 3. Oxygen acts as an acceptor in PbS (as it does in all of the lead salts) and exposures over this pressure range produced a maximum change in the electron population of 2.6×10^{13} cm^{-2}. This corresponds to a 23% reduction in the number of electrons in the conduction band. Although the R_H versus ρ plot does not reveal it, part of this oxygen uptake was reversible and pumping to low pressures always provided a partial restoration of the electron population.

We note in particular that the data points of Fig. 3 lie very precisely along a straight line whose slope gives a

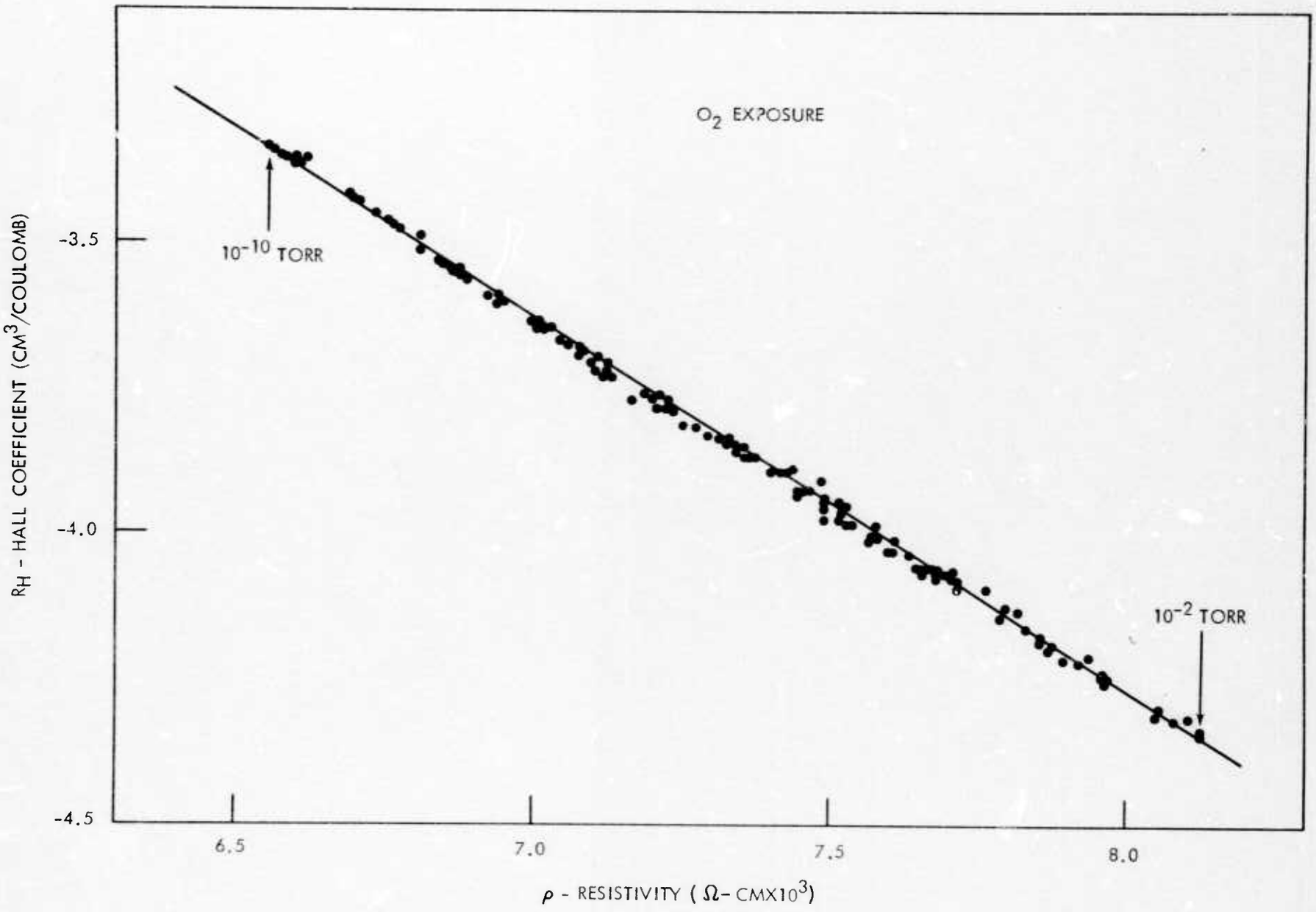
O_2 EXPOSURE
10^{-10} TORR
10^{-2} TORR
-3.5
-4.0
-4.5
6.5
7.0
7.5
8.0
R_H - HALL COEFFICIENT (CM^3/COULOMB)
ρ - RESISTIVITY (Ω- CMX10^3)

FIG. 3

mobility of 630 cm^2/volt-sec. This degree of linearity could not be achieved if the film contained more than one type of carrier, for that would require unrealistic variations in the carrier populations and/or mobilities. The data of Fig. 3 therefore constitute firm evidence that the film contains only a single carrier type having a constant mobility.

The very general results just cited are quite similar to the results previously reported for the lead chalcogenides,[1-6] and our observations remove a number of the fundamental ambiguities implicit in the previous studies. That is, we have for the first time eliminated the possibility that surface oxides or high background pressures of active gasses are responsible for major features of the adsorption such as the large changes in carrier population or the reversibility of the adsorption. However, we have also obtained a number of new results which indicate that the oxidation of the lead salts may be appreciably more complicated than previous transport studies would suggest.

Our observations show that the oxidation of PbS comprises at least four processes which can be distinguished on the basis of rate or reversibility. Our observations have revealed two reversible processes. One of these takes place at a very rapid rate and saturates in less than two minutes at pressures as low as 2×10^{-8} Torr. The second of these processes proceeds at a slower rate and saturates at an oxygen uptake which is dependent upon the oxygen pressure. We have also observed that there are one or more processes

which result in an irreversible oxygen uptake. The rate (or rates) of the irreversible adsorption have not been directly observable, but it has been found that the irreversible uptake saturates in an hour or less at a pressure of 6×10^{-6} Torr. We deduce from results in the literature[2,10,11] that there must be at least one more extremely slow process which produces the surface oxide layer which is known to form when PbS is exposed to the atmosphere.[10,11]

Each of the three chemisorption processes we observe in the low pressure regime can be associated with a specific component of the total change in the electron population. The irreversibly adsorbed oxygen is always responsible for a large fraction of the total electron population change and, of course, once saturation is reached this change is permanent. In the case of the reversibly adsorbed oxygen, the rapid process is responsible for only a small fraction of the total population change, while the slower process accounts for the balance. In a typical exposure run at 10^{-2} Torr, irreversible adsorption removes 10^{13} electrons per cm^2, the rapid reversible process removes 2×10^{12} electrons per cm^2 and the slower reversible process removes 1.4×10^{13} electrons per cm^2 for a total electron population decrease of 2.6×10^{13} cm^{-2}.

These results are illustrated by Figs. 4, 5 and 6. The curves of Fig. 4 were both obtained under the initial condition that the film contained no reversibly adsorbed oxygen, and the initial rapid uptake is readily apparent. For

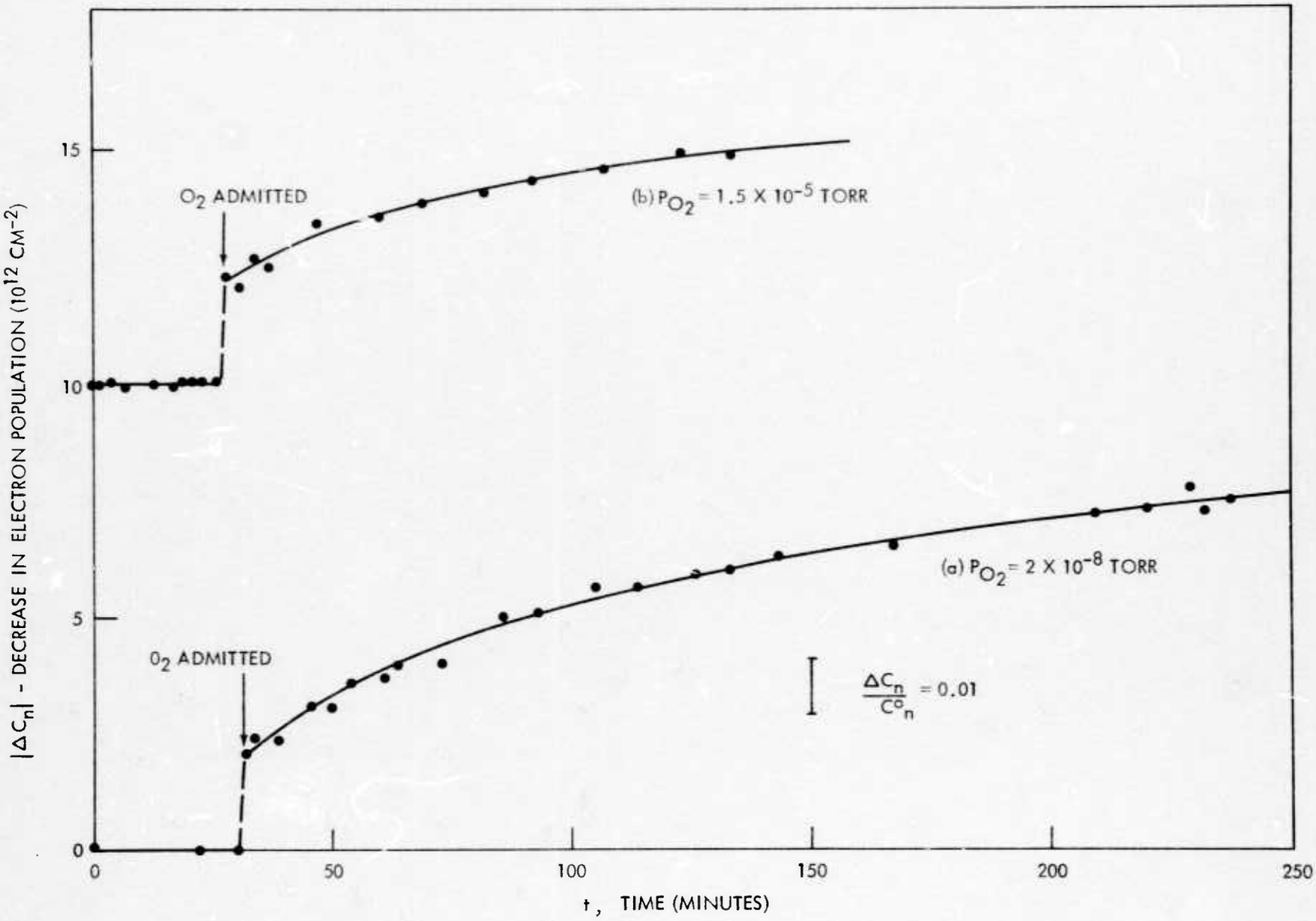
15
10
5
0
O_2 ADMITTED
(b) $P_{O_2} = 1.5 \times 10^{-5}$ TORR
(a) $P_{O_2} = 2 \times 10^{-8}$ TORR
O_2 ADMITTED
$\frac{\Delta C_n}{C^o_n} = 0.01$
0
50
100
150
200
250
t, TIME (MINUTES)
$|\Delta C_n|$ - DECREASE IN ELECTRON POPULATION (10^{12} CM^{-2})

FIG. 4

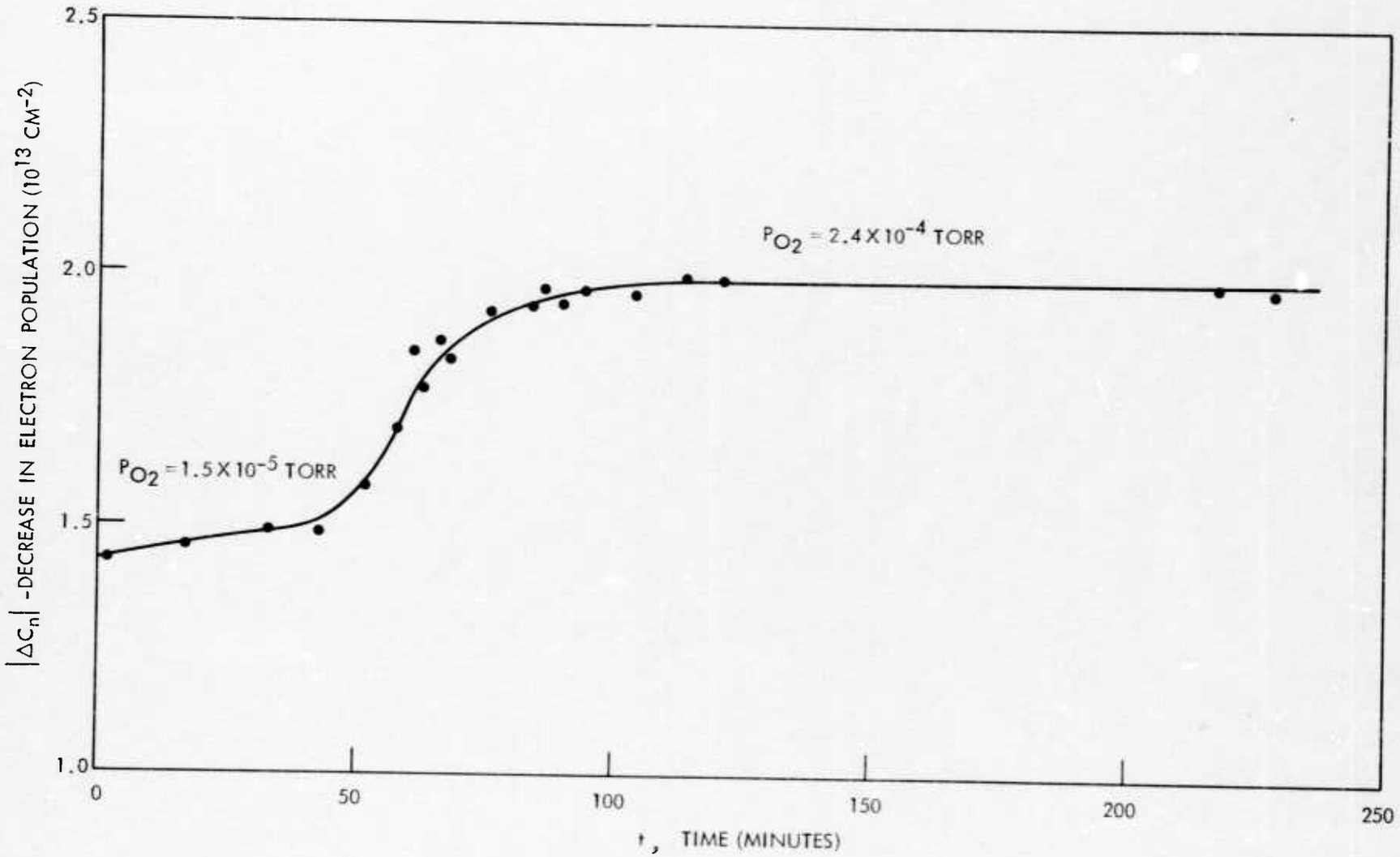
2.5
2.0
1.5
1.0
$|\Delta C_n|$ -DECREASE IN ELECTRON POPULATION (10^{13} CM^{-2})
$P_{O_2} = 2.4 \times 10^{-4}$ TORR
$P_{O_2} = 1.5 \times 10^{-5}$ TORR
0
50
100
150
200
250
t, TIME (MINUTES)

FIG. 5

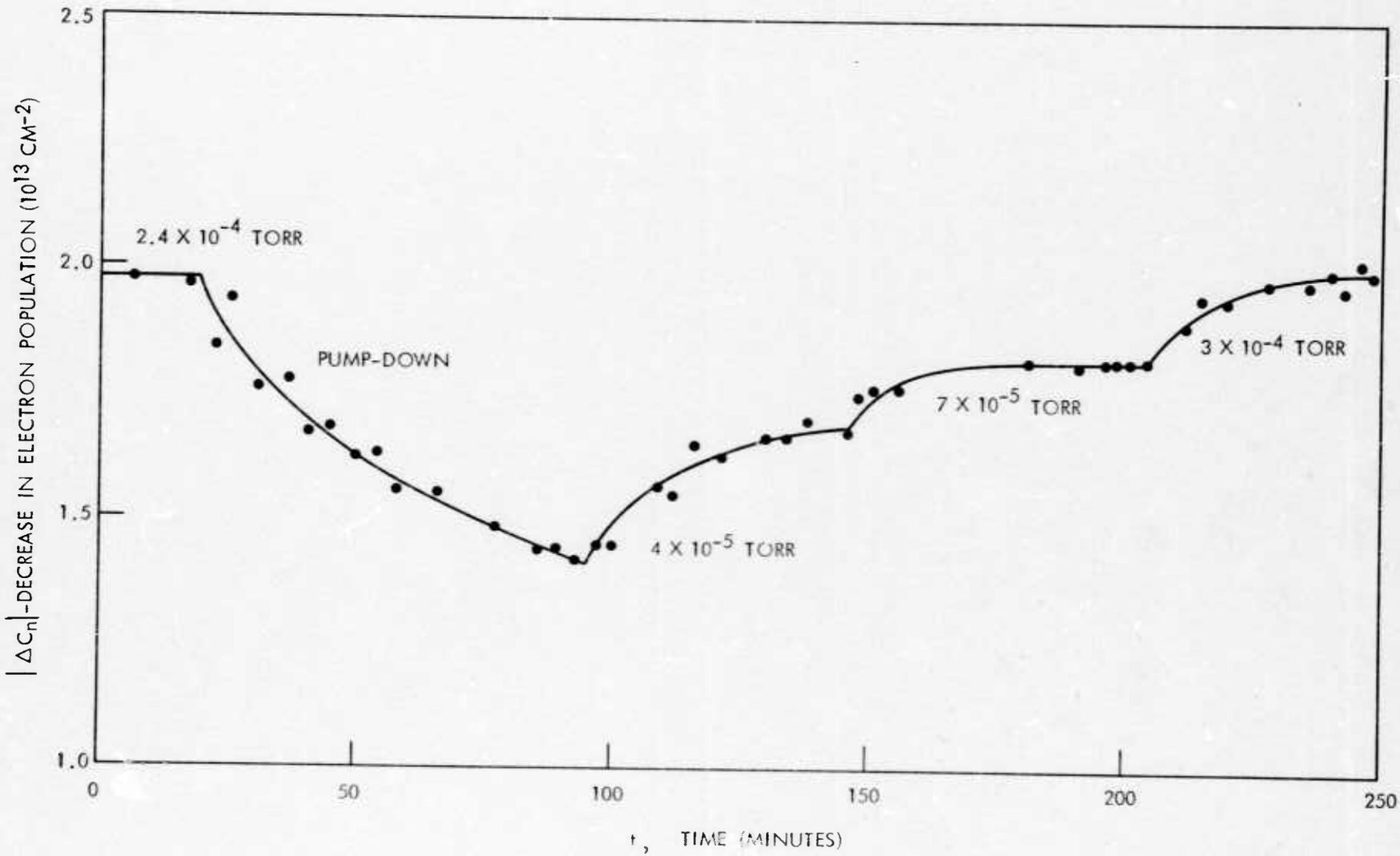
2.5
2.0
1.5
1.0
0
50
100
150
200
250
$|\Delta C_n|$-DECREASE IN ELECTRON POPULATION (10^{13} CM^{-2})
t, TIME (MINUTES)
2.4 X 10^{-4} TORR
PUMP-DOWN
4 X 10^{-5} TORR
7 X 10^{-5} TORR
3 X 10^{-4} TORR

FIG. 6

curve (a), the film had received no previous oxygen exposure and consequently contained no adsorbed oxygen at all. Curve (b) was obtained from the same film after the irreversible adsorption had been saturated and all of the reversibly adsorbed oxygen pumped off. We note that the amount of rapidly adsorbed oxygen was the same in both cases even though the oxygen pressure was 2×10^{-8} Torr in one instance and 1.5×10^{-5} Torr in the other. We observe, as well, that the subsequent slow uptake occurred at a faster rate in the initial exposure in spite of the fact that the pressure was higher than in the later exposure. Thus, the slow uptake rate in curve (a) is a composite of the rates of the irreversible and the slow reversible processes.

The curve of Fig. 5 is a continuation of Fig. 4(b). It illustrates that the slow process saturates at a constant oxygen pressure and a steady state electron population is achieved. The slow process clearly occurs at a pressure dependent rate, and we note that saturation was achieved relatively rapidly after the pressure was increased to 2.4×10^{-4} Torr.

In Fig. 6, we see an example of the desorption that occurs when the oxygen is pumped out of the experimental chamber. In this case, oxygen was re-admitted before all of the reversibly adsorbed oxygen was removed, and an initial rapid uptake was not observed. Evidently, the rapid process remains saturated until all of the oxygen associated with the slow process has been removed. The successive pressure increases indicated in Fig. 6 show that the saturation of the

slow process is pressure dependent.

These results were obtained at oxygen pressures which were five to ten orders of magnitude lower than those used in previous transport studies of oxygen chemisorption on lead chalcogenides,[1-6] and a direct comparison with the high pressure results cannot validly be made. It is unlikely, for example, that what we term the rapid process has ever been seen before. We believe, in fact, that the fast initial rate reported by Egerton and Juhasz[2] is actually a high pressure version of the slow rate reported here, and that their slow process is related to the growth of a surface oxide.

Our results, when viewed in the light of the known properties of PbS, raise serious questions about the validity of the diffusion models which have been proposed for the chemisorption of oxygen on PbS.[2,4,5] If we assume that the irreversible adsorption is associated with surface defect structure, then a diffusion model would require that the rapid uptake correspond to ionic adsorption at the surface and the slow uptake correspond to diffusion into the bulk. However, this would seem to leave no mechanism to explain the very slow uptake that has been observed to affect the carrier concentration in previous transport studies. Furthermore, it would seem much more likely that a surface mechanism would display the observed reversibility and pressure dependence.

It would seem that any proposed model would have to be consistent with the formation of a surface oxide in order to be entirely plausible, and the diffusion model does not

appear to be consistent with the known facts. Low-energy electron diffraction (LEED) studies[11] tell us that a 48 Torr-hour exposure to oxygen results in approximately 0.1 monolayer of amorphous oxide on the surface and that exposure to atmosphere produces a thick surface layer of amorphous oxide. In previous transport studies, a 48 Torr-hour exposure was exceeded in the first four minutes at atmospheric pressure, and the entire oxygen uptake observed in this time would have to remain on the surface in order to be consistent with the LEED results. Also, the diffusion model makes no provision for the formation of a heavy surface oxide. The oxide formation would necessarily affect the carrier population in the film and it would undoubtedly contribute to the slow change in carrier population that has been reported to occur in air.

The difficulties in explaining oxygen adsorption on the lead salts have arisen primarily because of the very large charge exchange which has been associated with the observed changes in carrier population. The primary virtue of the diffusion model is that, by distributing this excess charge throughout the bulk, it avoids the necessity of extreme band-bending. We believe, however, that surface processes exist which can explain all of the data at hand without creating the extreme band-bending which is so objectionable. We are currently investigating a category of surface processes which may have the desired characteristics.

4. Analysis of Transport in Two-Carrier Films (Experimental, Theoretical: R. N. Lee)

One of the prominent results of chemisorption studies on IV-VI films has been that the carrier mobilities remain unchanged by relatively large variations in the carrier populations.[1-6] Interpretation of transport data is considerably simplified when the carrier mobilities are constant and this feature of the data has been explicitly used in previous interpretations of the effects of chemisorption on the electrical properties of IV-VI films.[1-6] Previous analyses have all assumed specific carrier concentration profiles in the films,[1-6] however, and the fundamental simplifications provided by the constant carrier mobilities have not been used to the best advantage.

We will now show that when the carrier mobilities are constant, the transport data provide a clear physical picture of the changes occurring in a two-carrier film. We will show that transport data can tell us the number of carriers of each type in the film and give us the change in the number of ionized dopants as well as the degree of spatial overlap of the two carrier types. This is the maximum information which may be derived from the transport data, and it is obtained without introducing assumptions as to the carrier concentration profiles within the film.

In general, the conductivity σ and the Hall coefficient R_H in two-carrier layered films are governed by the relatively complicated Petritz[12] equations (we take the carriers to be electrons and holes for purposes of discussion).

$$\sigma d = e\int_0^d \mu_p(z)p(z)dz + e\int_0^d \mu_n(z)n(z)dz \ , \tag{1}$$

$$R_H\sigma^2 d = e\int_0^d \mu_p^{\,2}(z)p(z)dz - e\int_0^d \mu_n^{\,2}(z)n(z)dz \ , \tag{2}$$

where d is the film thickness and z is the distance from the surface.

When the carrier mobilities are constant, these relations simplify to

$$\sigma d = e\mu_p C_p + e\mu_n C_n \ , \tag{3}$$

$$R_H\sigma^2 d = e\mu_p^{\,2} C_p - e\mu_n^{\,2} C_n \ , \tag{4}$$

where

$$C_p = \int_0^d p(z)dz \text{ and } C_n = \int_0^d n(z)dz \tag{5}$$

are the hole and electron populations (total number in the film per unit film area), respectively.

We stress that the use of the carrier populations rather than the carrier concentrations avoids the problems associated with guessing the carrier concentration profiles p(z) and n(z) in (1) and (2). In fact, it is clear from the equations that R_H and σ provide no information whatever about the spatial distribution of the carriers within the film.

Inversion of (3) and (4) gives the carrier populations directly in terms of the experimentally determined quantities. That is,

$$C_p = \frac{\sigma d}{e\mu_p} \frac{(R_H\sigma+\mu_n)}{(\mu_p+\mu_n)} \quad , \tag{6}$$

$$C_n = \frac{\sigma d}{e\mu_n} \frac{(\mu_p-R_H\sigma)}{(\mu_p+\mu_n)} \quad . \tag{7}$$

The maximum possible information is extracted from the resistivity and Hall data when we relate the carrier populations to the number N_D of ionized dopant atoms added to the film. This is accomplished by invoking electrical neutrality of the film,

$$eC_p^o - eC_n^o = q_D N_D + eC_p - eC_n \tag{8}$$

where C_p^o and C_n^o are the initial carrier populations and q_D is the charge on the ionized dopant atom. We may then use 6, 7 and 8 to write N_D in terms of experimentally determined quantities;

$$N_D = \frac{d}{q_D\mu_n\mu_p}[(R_H^o\sigma_o^2 - R_H\sigma^2) + (\mu_n - \mu_p)(\sigma_o - \sigma)] \tag{9}$$

where R_H^o and σ_o are the values obtained for the initial condition of the film.

Thus, we see that measurements of R_H and σ provide a direct physical picture of the film. Plots of C_p and C_n versus N_D or of C_p, C_n and N_D versus other experimental variables (e.g. time or gas pressure) present the measurements in a highly intuitive way. Such population plots offer great advantages over the commonly used R_H versus ρ plots[1,2,4,5] in the interpretation of the data, for the relationship between the form of the R_H versus ρ curve and the behavior of the carriers is not usually readily apparent in a two-carrier regime.

The transverse magnetoresistances may also be expressed in terms which simplify interpretation. It has been observed that there is an anisotropy in the transverse magnetoresistance in IV-VI films that is a function of gas adsorption,[3,6] but the basic reasons for this anisotropy have not been adequately explained in the context of the observed constant carrier mobilities.

The expression obtained by Petritz[12] for the transverse magnetoresistance with the magnetic field perpendicular to the film is

$$\frac{\Delta\rho}{\rho H^2} = \frac{e}{\sigma d}\sum_k \int_o^d n_k(z)\mu_k^3(z)dz - (\sigma d)^{-2}\left[\sum_k \int_o^d q_k n_k(z)\mu_k^2(z)dz\right]^2. \tag{10}$$

Although Petritz did not derive an expression for the case of the magnetic field parallel to the film, McLane has recently obtained an expression for this quantity.[6]

$$\frac{\Delta\rho}{\rho H^2} = \frac{e}{\sigma d}\sum_k \int_o^d n_k(z)\mu_k^3(z)dz - (\sigma d)^{-1}\int_o^d \frac{\left[\sum_k q_k n_k(z)\mu_k^2(z)\right]^2}{\left[e\sum_k n_k(z)\mu_k(z)\right]^2}dz. \tag{11}$$

If we again assume a two-carrier system with constant mobilities, equations 10 and 11 reduce to

$$\frac{\Delta\rho}{\rho H^2} = \frac{\mu_p\mu_n e}{(\sigma d)^2}(\mu_p + \mu_n)^2 C_n C_p \quad , \tag{12}$$

and

$$\frac{\Delta\rho}{\rho H^2} = \frac{\mu_p \mu_n e}{\sigma d}(\mu_p + \mu_n)^2 \int_o^d \frac{p(z)n(z)dz}{e(\mu_p p(z) + \mu_n n(z))} \quad . \qquad (13)$$

Written in this manner, the equations immediately clarify the physical reasons for the anisotropy in the transverse magnetoresistance. The perpendicular field magnetoresistance depends only on the total number of carriers of each type in the film, and is independent of the carrier concentration profiles. The parallel field magnetoresistance is, however, a measure of the spatial overlap of the two carrier types. The parallel magnetoresistance is therefore expected to be less than the perpendicular magnetoresistance in layered films on very general grounds.

It is important to note that these expressions are both zero if there is only one carrier type and that this is an artifact of the constant mobility assumption. In actuality, of course, there will be a magnetoresistance in a homogeneous single-carrier film due to the energy dependence of the scattering time. Such an energy dependence is inconsistent with the strict insistence that the carrier mobilities be constant, however, for it would imply that a variation in carrier concentration would result in a change in mobility.

If we had maintained a distinction between the conductivity mobility $\langle\mu\rangle$, the Hall mobility $\langle\mu^2\rangle^{1/2}$, and the magnetoresistance mobility $\langle\mu^3\rangle^{1/3}$, Eq. 12 would also contain terms in C_1^2, C_2^2, and C_1C_2 which go to zero when the three mobilities are equal. (i.e. when there is no energy dependence of the scattering time.)

Analogous energy dependent terms would appear in Eq. (13). In practice, these terms will not be zero and they cannot easily be subtracted from the data. Thus, equation 12 may not be used quantitatively with any confidence.

The size of the energy dependent coefficients in the magnetoresistances may be estimated by observing the variation in the measured magnetoresistances in the single carrier regime. If the magnitudes and dependence on carrier population in this region are small compared with the variation in the two carrier regime, it is probably safe to make a qualitative interpretation of the behavior in the latter region.

The population plot of Fig. 7 provides an illustration of the great utility of such plots. In this hypothetical example, we presume that an n-p junction device is fabricated by ion implanting acceptors in an n-type film and that the device fails after a certain period of operation. We see that the population plot clearly identifies the failure mode as being due to electromigration. The line segments AB and A'B' correspond to the formation of the junction. As the donors are implanted, the electron population decreases and the hole population increases until implantation is terminated (points B and B'). Operation of the device results in the reduction of both populations by equal amounts, but the amount of ionized dopant remains unchanged during this time (line segments BC and B'C'). Such behavior of the carrier and dopant populations could only be the result of the diffusion of dopant across the junction and the consequent mutual annihilation of electrons and holes as the junction becomes smeared out. Confirmation of this interpretation

would be provided by an increase in the parallel magnetoresistance during the decay of the carrier populations.

Alternate failure modes would have produced their own distinctive population plots. For example, failure due to poisoning by donor impurities diffusing from the surface of the device would result in a population plot of the type illustrated in Fig. 8. These two failure modes would also produce different R_H versus ρ curves, it is true, but only the population plots clearly identify the mechanism at work.

The many applications which can be envisioned for this analytical technique indicate that it will prove to be invaluable both as a tool for device diagnostics and as an aid in the investigation of the fundamental phenomena underlying device technology. This work is being prepared for publication.

5. Appearance Potential Spectroscopy of Surfaces (Experimental: B. V. Kessler and R. N. Lee)

a. The method: It is important to know the chemical constituents of the PbS surface and how they are chemically bonded, answering such questions as: Is oxygen present and what sort of Pb;O;S structures are present? Is free lead present, etc? Appearance potential spectroscopy[13] (APS) is an extremely simple method of surface chemical analysis, not requiring complicated electron energy analyzers. Only the soft X-ray de-excitation of surface atoms, bombarded by an incident electron beam, is measured. (More accurately, one measures the slope of the soft X-ray yield versus electron beam energy, using

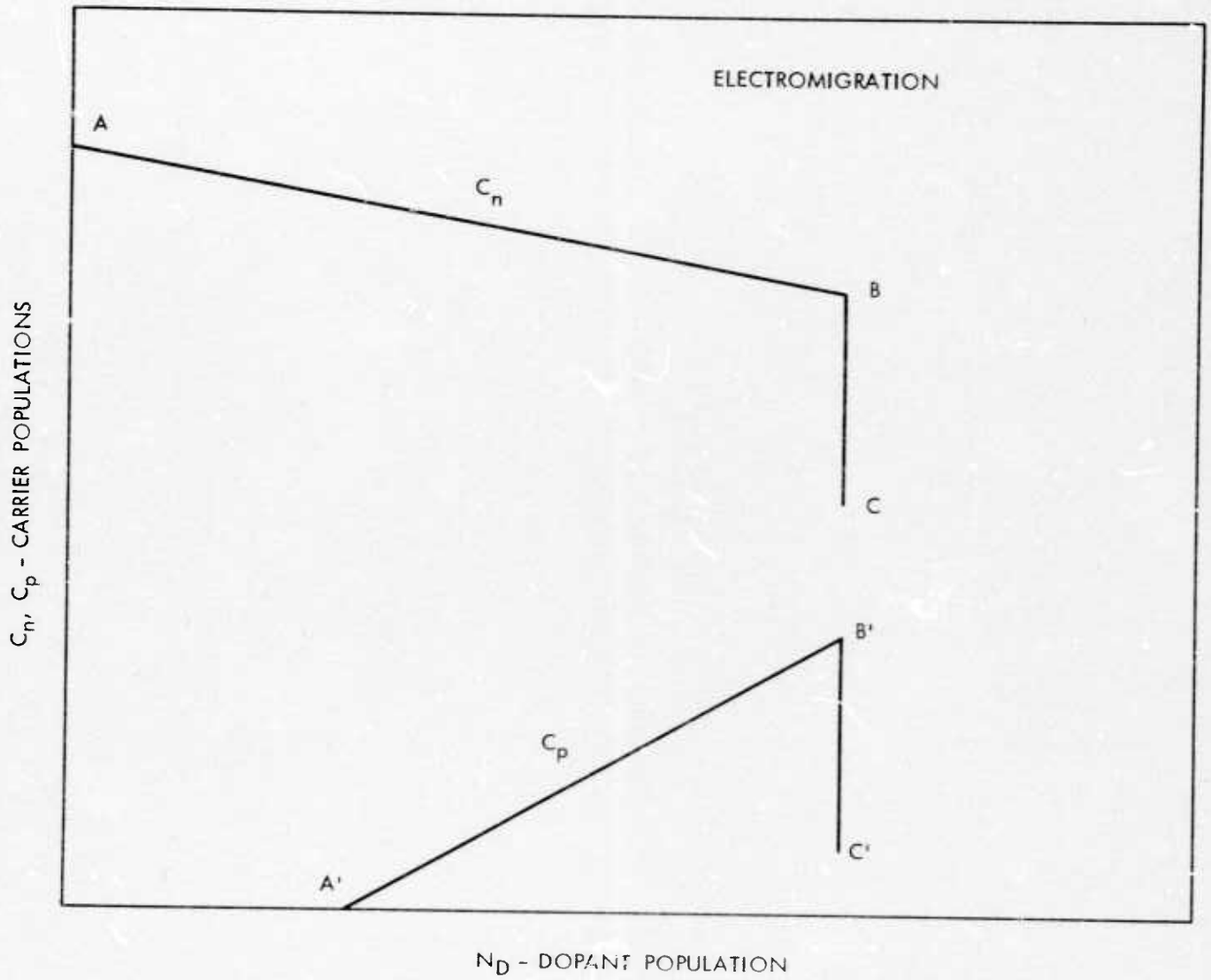
ELECTROMIGRATION
A
C_n
B
C
B'
C_p
C'
A'
C_n, C_p - CARRIER POPULATIONS
N_D - DOPANT POPULATION

FIG. 7

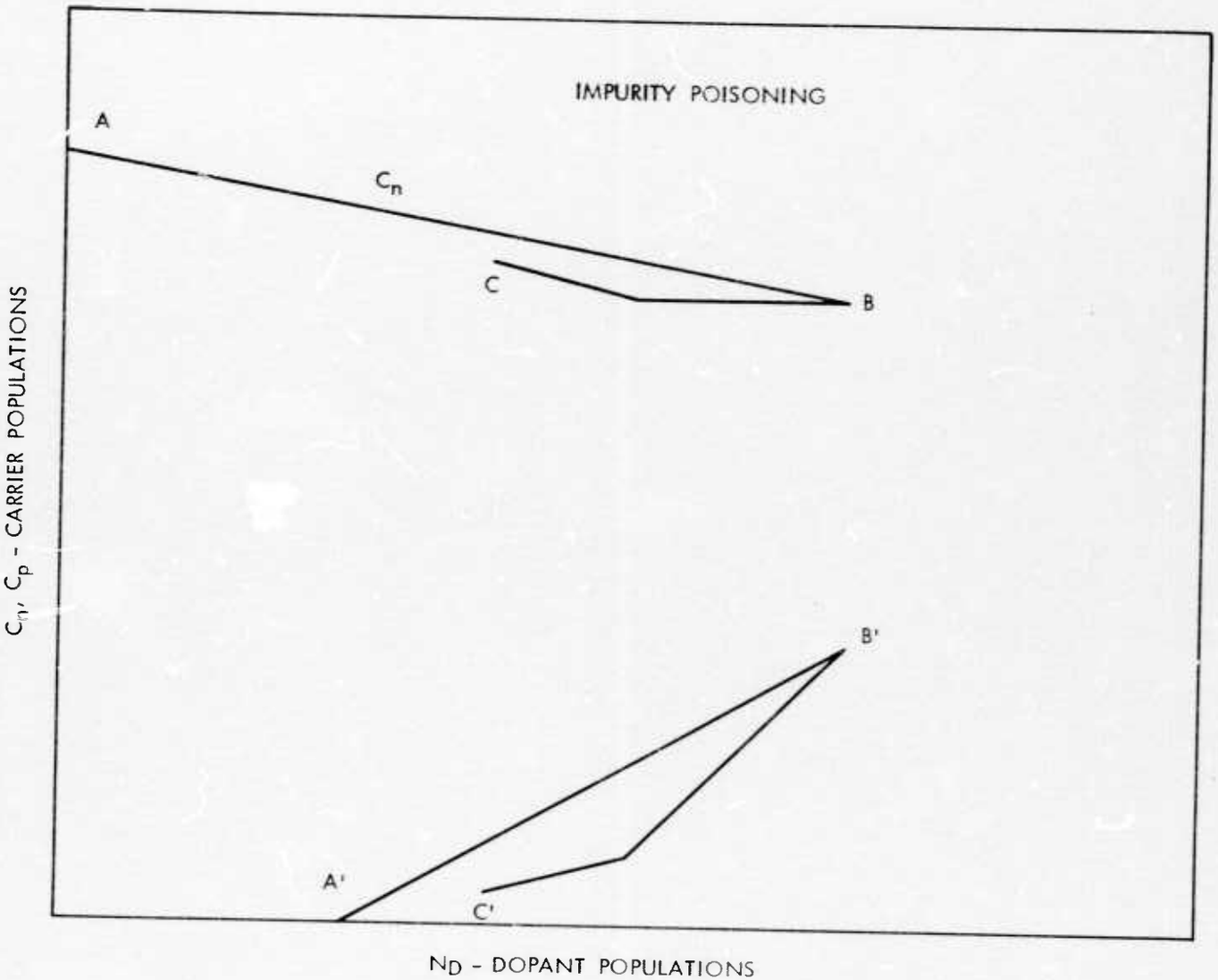
IMPURITY POISONING
A
C_n
C
B
B'
A'
C'
C_n, C_p - CARRIER POPULATIONS
N_D - DOPANT POPULATIONS

FIG. 8

modulation techniques.) Specific chemical constituents have, of course, specific core levels, and the chemical shift of these provides information about the chemical environment of these atoms. At threshold for excitation of an inner core electron to the Fermi level, there is a small but sudden increase in the soft X-ray yield which then produces a large signal (Δ Yield/Δ Energy).

APS has been attempted[14] with III-V semiconductors but considered impractical there because the APS signals obtained were several orders of magnitude smaller than with transition metals. The reason for this small signal in semiconductors is that APS signals depend on the square of the state density N_F at the Fermi level. However, in the degenerate IV-VI semiconductors N_F is much higher than in non-degenerate III-V semiconductors so that the method may well be feasible.

APS will be applied first to the TiNi alloys, which have high N_F, to test the APS spectrometer, which we have built, and to examine chemical shifts at the transition temperature of this material, a second order phase transition which is thought to be non-structural.

Although intended primarily as a surface diagnostic tool, the APS technique is new enough to be of some interest in itself. The reasons, for example, why APS signals are not seen with some 4d and 5d transition metals and alloys are not yet understood. It also remains to work out the application of the APS method to materials used for infrared device technology.

b. The chemical shift: With APS, surface impurities can be identified with good sensitivity. APS also measures the chemical shift from which one can deduce information about the structure of the surface. This is done by using an inner-core-electron energy level as a 'window' in which to sense the charge in the valence electrons of a surface atom since a change in the valence state of a surface atom results in a variation of the inner core energy level and is revealed in the APS electronic spectra.

The origin of the chemical shift can be illustrated in an idealized example. For an atom, consider only the deepest inner K-shell electron and the outermost valence electron, ignoring the intermediate electrons. For simplicity assume the valence electron has a spherical charge distribution. Figure 1 then delineates the electrostatic potentials which result. Note that the spatial extent of the valence electron is of the order of 1 Å whereas the inner core electron radius is much smaller, e.g. can be as small as 0.01 Å for a high Z ion. Now it is the valence electronic charge distribution which partakes in chemical interactions with neighboring ions. The effect therefore of a variation in say the magnitude of the assumed spherical valence charge is to translate the nuclear attractive potential which binds the inner core electron upward or downward as in Fig. 9. For example, should the ion of interest become surrounded say by more electronegative neighbors the valence charge would be diminished and the positive potential due to this charge would be decreased, effectively lowering the entire nuclear

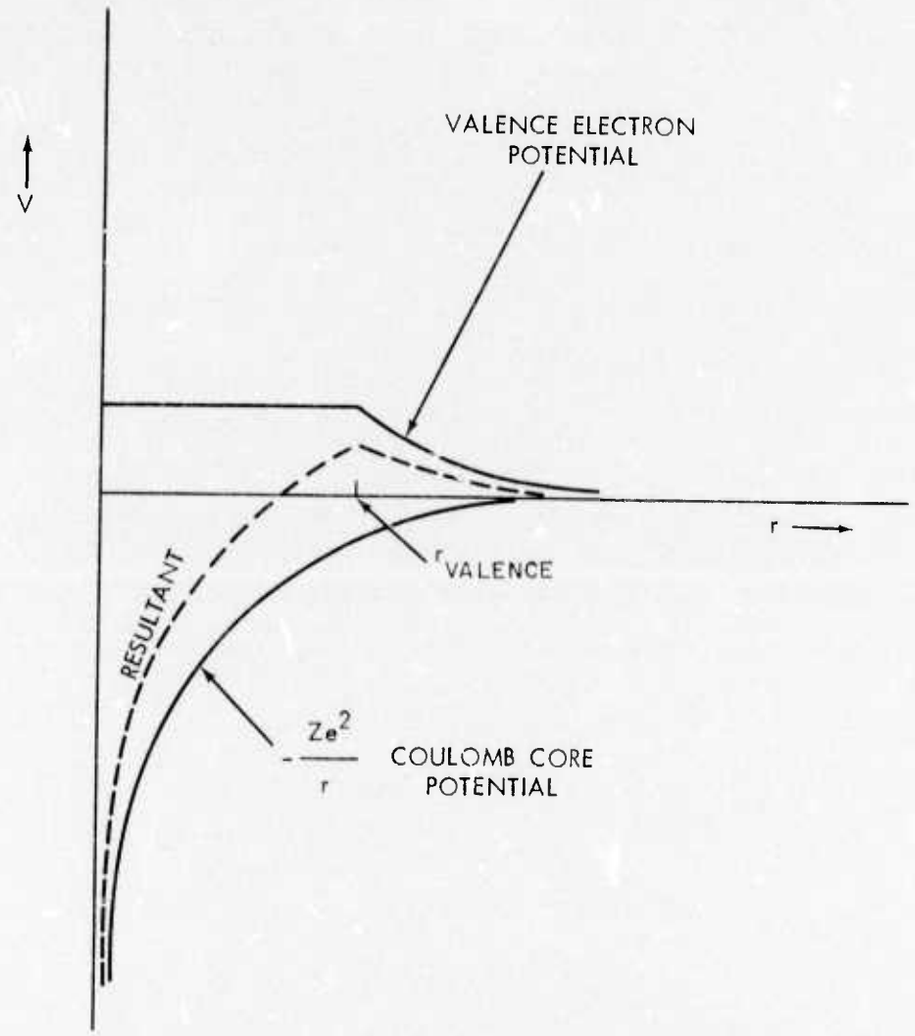

FIG. 9 POTENTIAL OF CORE ELECTION AS MODIFIED BY "SPHERICAL SHELL" VALENCE ELECTRON

coulomb potential curve seen by the inner electron and increasing its binding energy. This sensitivity of the inner-core-electron binding energy to the disposition of charge of the outer valence charge is termed the chemical shift.

The foregoing simplified model would seem to indicate that a given change in valence charge magnitude would always lead to the same chemical shift. Such is not the case in reality; the valence charge is not removed to infinity as assumed above but is redistributed amongst neighboring ions in accordance with the particular nature of the ionic-valence bonding. There is also an interaction energy due to some wave function overlap of the valence and inner core electrons which changes as the valence charge redistributes. Also the valence electron in general does not have spherical symmetry.

There is therefore a chemical shift in going from a free atom to the liquid or solid state. There are also chemical shifts when ionic environment in a crystal is changed by vacancies, impurities, or order-disorder phase transitions. From the chemical shift one may try to deduce the location and identity of surrounding ions and correlate this structural information with device figures of merit and performance.

c. Features of APS. APS is the threshold measurement for electronic excitation of an inner core electron of a surface atom to the Fermi level. This threshold is sharp when both the inner and Fermi levels are well-defined. At threshold both the incident and the inner core electron end up at the Fermi level (leaving a localized core hole). Since

this transition involves the disposition of two electrons, the excitation probability depends on the square of final state density, i.e. at the Fermi level.

Plasmon-aided de-excitation can also occur. This produces a plasmon satellite structure in the output data, with separations determined by the plasmon energy. Plasmon satellites are especially strong in low Z materials where the core size is such as to couple better with the electron density fluctuations.

In APS the experimental procedure probes only surface rather than bulk atomic phenomena for the following reason: The moderate energy electrons used (200 to 2,000 eV) do penetrate many monolayers. But the incident electron loses some energy traversing each layer and, if at threshold energy at the surface, is below threshold after penetrating a few atomic layers.

d. Experimental Setup. The experimental apparatus is shown schematically in Fig. 10. Accelerated electrons from a heated tungsten filament, F, strike the anode, S, which serves as the sample under study. As the anode potential is slowly increased there is a certain incident electron energy at which the accelerated filament electrons are energetically capable of exciting an inner core electron of a surface ion to the Fermi level; at this threshold both the incident electron and the inner core electron end up in the first unoccupied states above the Fermi level.
The threshold electron-excitation-level for a core level of a given surface ion constitutes the primary data of the experiment.

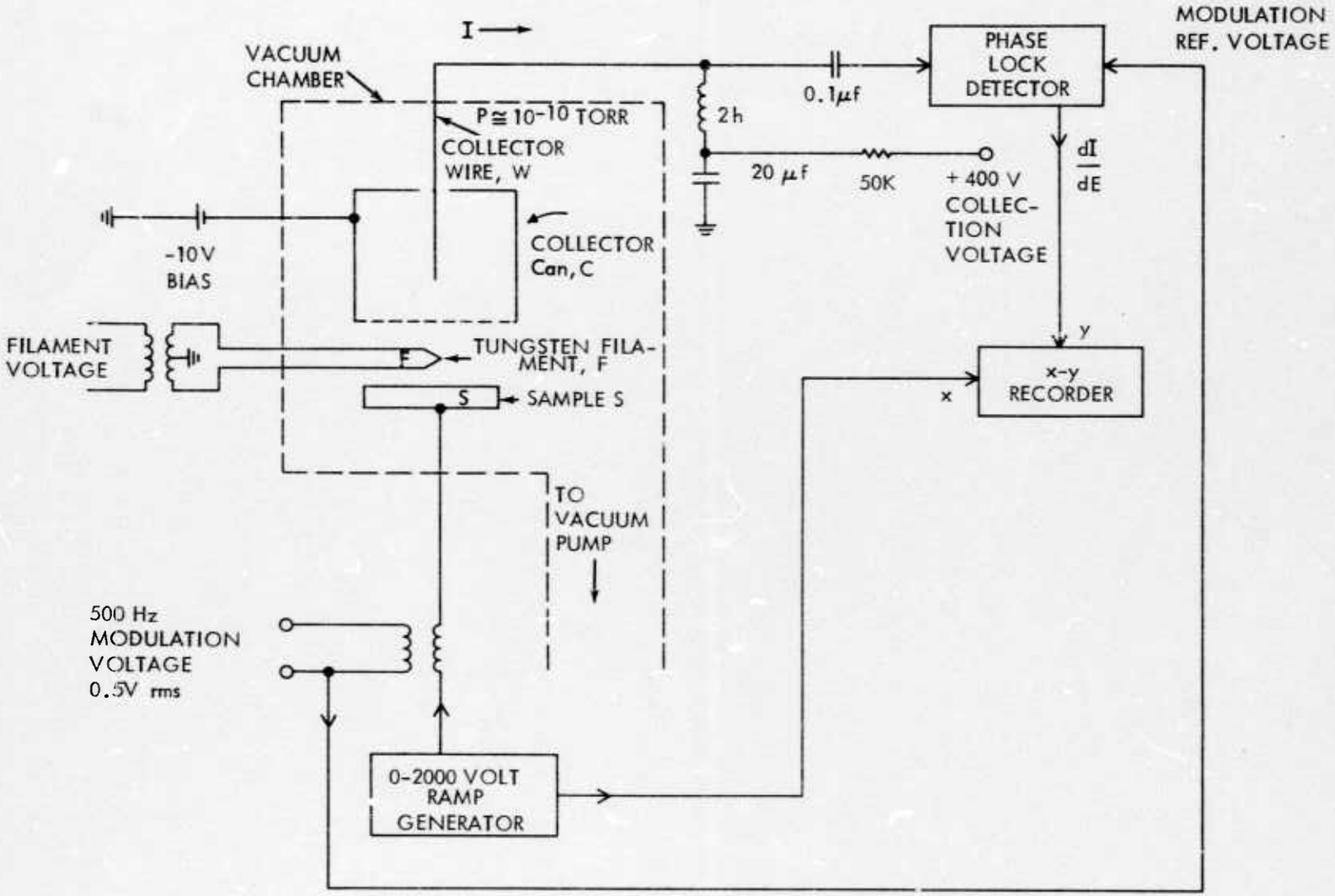

FIG. 10 APPEARANCE POTENTIAL SPECTROMETER AND AUXILIARY ELECTRONICS.

De-excitation, i.e. filling of the core vacancy occurs both by radiative and Auger processes. Although the latter dominates for the 1 keV energies in question it is nevertheless the gross soft x-ray yield which is measured in APS; complex and expensive energy analysers for decay products are thus not needed.

The soft x-rays pass through a grid in front of a collection can, C, and generate photoelectrons upon collision with the walls of the can, which electrons are, in turn, collected by a wire, W, held at a positive potential. Auger and filament electrons are kept out of the collector can by applying a negative bias voltage to the can.

The experiment is conducted as follows: As the sample voltage is increased so that some new deeper lying core electron energy level can just barely be excited up to the Fermi level, the sudden "appearance" of a small increase in x-ray yield is a measure of the core electron energy level. This small but sudden increase is more easily seen amidst the large but slowly varying soft-x-ray background yield (from all other radiative de-excitation channels) by resorting to electronic differentiation of the collector current. This is done in the usual manner by superimposing a "wiggle" frequency upon the sample potential and using synchronous detection by phase lock instrumentation.

A basic limit of energy resolution is the energy spread of the incident electron beam due to the voltage drop along the filament and the thermal spread. The Auger lifetime of the core hole also provides a basic linewidth.

An APS apparatus can be rather easily modified to an Auger Appearance Potential Spectroscopy (AAPS) apparatus by adding electron collection plates nearby the sample. Although energy analysis of Auger electrons is not performed it still remains a "spectrometer" in that inner-core energy levels can be determined. Because Auger de-excitation dominates in the soft x-ray energy range of interest these signals would be more easily detected. APS and AAPS are complementary techniques in the sense that overlapping spectral lines from two different surface elements in say AAPS would, in general, be well separated in APS and vice versa.

An ultrahigh vacuum system has been built and a pressure of 2.6×10^{-10} Torr reached after a 200°C bakeout. An APS spectrometer[15] has been built on a Varian vacuum flange and is shown in Fig. 11. The electronic voltage sweep is currently being designed and constructed. The schedule is to try a transition metal first to check out spectrometer calibration and sensitivity, and then to proceed to the lead salts. The chemical shift for say PbS will be established by measuring an N shell core level both before and after exposure to oxygen.

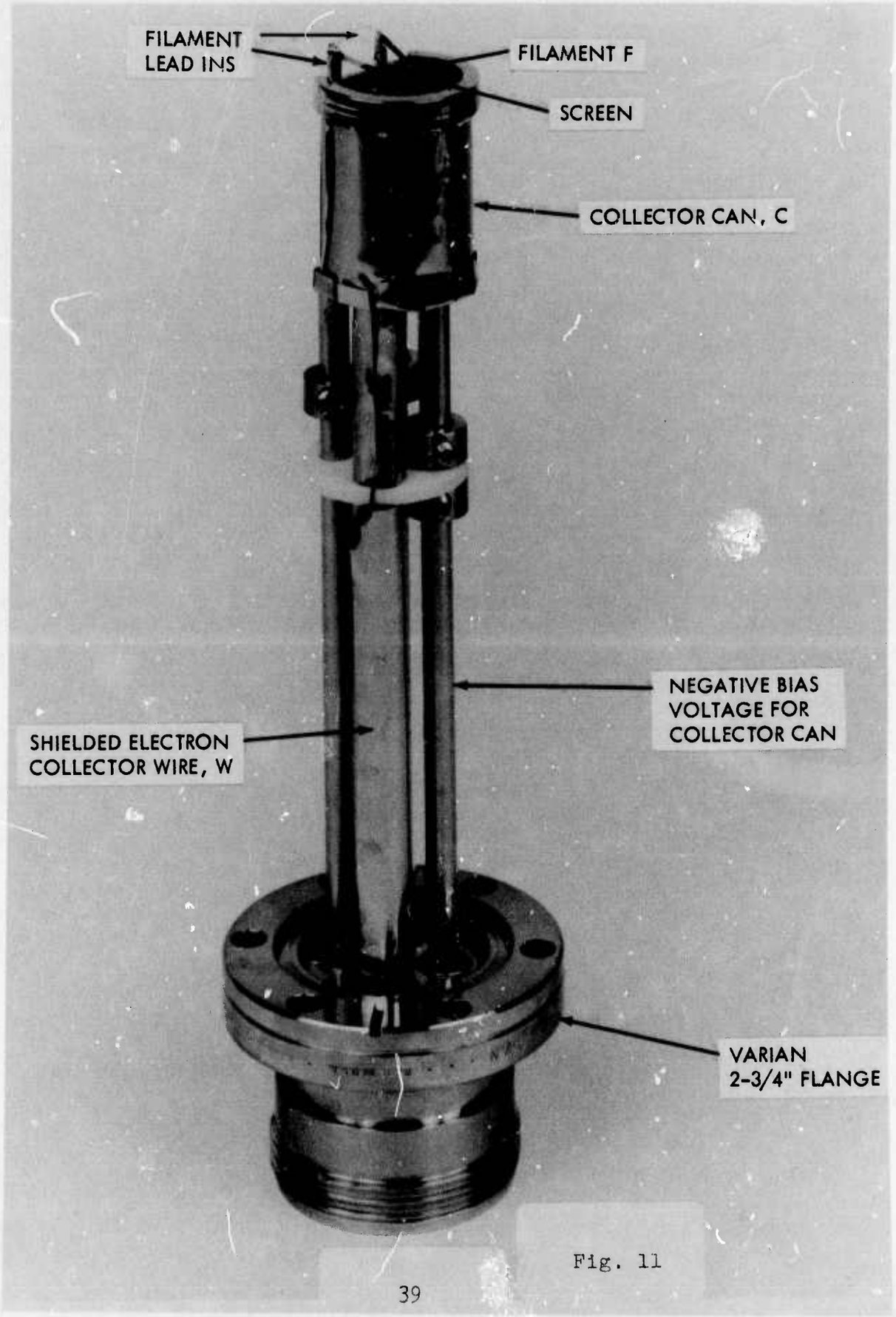
FILAMENT
LEAD INS
FILAMENT F
SCREEN
COLLECTOR CAN, C
NEGATIVE BIAS
VOLTAGE FOR
COLLECTOR CAN
SHIELDED ELECTRON
COLLECTOR WIRE, W
VARIAN
2-3/4" FLANGE

Fig. 11

6. Carrier Scattering in Semiconductors by Screened Surface Charges (Theory: R. F. Greene and John Malamas*)

Early work[19] by Greene and O'Donnell in 1966 had established that surface charges, e.g. in chemisorption bonds, provide the dominant surface scattering mechanism at fairly well-prepared semiconductor surfaces. Several important problems remained unsolved, however, until the present work:[16]

a. The actual form of the screened potential of a partly random array of surface charges was unknown in 1966, so that an arbitrary Yukawa-type of scattering potential had to be used then. The actual three-dimensional form of the space charge potential of such an array was determined finally in an earlier part of this program[20] and it is this realistic potential that is used in the present work.[16]

b. Dielectric image effects were omitted in the Greene-O'Donnell calculation.[19] This force, which repels carriers from regions of lower polarizability, has been included in the present calculation, where it is shown to decouple carriers appreciably from surface scattering potentials.

c. Surface charge densities are commonly high enough for several scatterers to lie within an electron wavelength, resulting in strong interferences between scattered waves. This was ignored in the Greene-O'Donnell calculation, but is treated exactly now. This is done by treating the entire screened array as a single scatterer, whose detailed arrangement is represented in the scattering rate by the structure

---

*Army Night Vision Laboratory (not supported under this contract).

factor S of the array. Numerical values of the Fuchs reflectivity factor are presented, for various material parameters, and as a function of the angular coordinates of electrons leaving the surface. Complete details of this calculation are given in the enclosure (1), which is a preprint of reference 16.

7. Surface Transport (Theory: R. F. Greene)

Surface transport calculations, requiring quantitative values of the Fuchs carrier reflectivity and its angular dependence, provide values of surface mobility, surface Hall coefficient, and surface magnetoresistance, with which surface scattering models can be tested against experiment. Improvements are needed in the transport theory, principally because the standard surface transport theory does not handle the energy dependence of bulk scattering time, which is crucial for the surface galvanomagnetic properties. We are making these improvements in the theory and carrying out the evaluation of the surface galvanomagnetic coefficients numerically.

8. Chemisorption Thermodynamics - Surface Scattering Connection (Theory: R. F. Greene)

We have made an important breakthrough in the theory of semiconductor surfaces, with the discovery of a direct relation between the adsorption isotherm of charged chemisorbed atoms and the surface scattering produced in the semiconductor. (A preliminary form of this result has been published in Thin Solid Films[17] and a final form in Surface Science[18]). This discovery makes it possible for the first time to use

chemisorption data to clarify transport phenomena and vice versa, and should greatly increase the ability of scientists to test models of surface structure.

This breakthrough was an unexpected result of our investigation of interference effects in surface scattering of carriers in semiconductors. Using the Born approximation, we found that these interference effects could be expressed in terms of the structure factor S which represents the arrangement of the surface scatterers. We used the fact that S is the Fourier transform of the pair correlation function which represents the effects of interaction between adsorbed atoms in the statistical thermodynamics of chemisorption. The non-ideal behavior of the adsorbed gas, as measured by its deviation from the Langmuir isotherm, is directly related to the interference effects in the surface scattering produced by these adsorbed atoms. Both the deviations from the Lanmuir isotherm and the scattering interferences are obtainable from experiment, and a test of the theory will be attempted experimentally with various gases on IV-VI semiconductor surfaces. The new theoretical relation can be written in terms of the Fuchs reflectivity p (which determines the surface mobility) as follows:

$$p = p_{random}\,(kT/\bar{n}(1-\bar{n}))(\partial\bar{n}/\partial g)_T$$

where p_{random} is the calculated value of p for a random array, n is the mean occupation number of a surface site (coverage) and g is adion chemical potential, obtainable from the overpressure. Complete details are given in enclosure (2) which is a preprint of reference 18.

9. Theory of Chemisorption Isotherms on Semiconductors

(Theory: R. F. Greene and C. Richmond*)

Work has begun on the statistical thermodynamic calculation of chemisorption isotherms for various gases on semiconductors, emphasizing the interactions between adions, and the formation of space-charge layers. Instead of the familiar adsorption isotherm of Langmuir for the case of no interaction between adions, which can be written in the form

$$\bar{n} = (1 + \exp((\varepsilon_o - g)/kT)^{-1}$$

(random arrangement), we show that chemisorption with charge transfer produces a non-Langmuir isotherm of the form

$$\bar{n} = (1 + \exp((\varepsilon_o - g + \tfrac{1}{2}e\phi_{ps}(\bar{n}))/kT)^{-1}$$

where ϕ_{ps} is the band-bending potential, with which we express the adion interaction. Numerical evaluation shows that this extra electrostatic interaction depresses the coverage $\bar{n}$. Extensions of the theory are being made to take into account partial ionization of the chemisorbed atoms, and to treat the interaction by the Bragg-Williams and Bethe-Peierls methods.

10. Dielectric Image Force Theory (Theory: R. F. Greene)

Our scattering theory has shown that the dielectric image force plays an important role in surface scattering. The dielectric image force is also known to be important in

---

*Not supported under this contract.

heterojunction tunnelling and in surface recombination effects. Nevertheless, the theory remains in an unsatisfactory state. The present classical theory diverges as the electron approaches the surface, and the sign of the force itself is unknown for holes.

We have begun a quantum treatment of the dielectric image force, introducing dispersive lattice optical modes explicitly and so removing the classical divergence. Many body techniques are being employed to treat the nearly filled band case.

REFERENCES

1. M. H. Brodsky and J. N. Zemel, Phys. Rev. 155, 780 (1967).
2. R. F. Egerton and C. Juhasz, Thin Solid Films 4, 239 (1969).
3. M. H. Brodsky and R. B. Schoolar, J. Appl. Phys. 40, 107 (1969).
4. G. McLane and J. N. Zemel, Thin Solid Films 7, 229 (1971).
5. A. Cepeda, G. McLane, and J. N. Zemel, J. Vac. Sci. Tech. 9, 239 (1972).
6. G. McLane, J. Appl. Phys. (to be published).
7. M. Paic, V. Paic, K. Duh, and J. N. Zemel, Thin Solid Films 13, 204 (1972).
8. H. Holloway and E. M. Logothetis, J. Appl. Phys. 42, 4522 (1971).
9. J. N. Zemel: University of Pennsylvania Progress Report, ARPA Contract N60921-70-C-0251 1972 (the U. of Penn. portion of this Progress Report).
10. D. C. Johnson and A. U. Macrae, J. Appl. Phys. 37, 2298 (1967).
11. R. N. Lee, J. de Physique 29 Suppl. to No. 11-12, C4-43 (1968).
12. R. L. Petritz, Phys. Rev. 110, 1254 (1958).
13. J. E. Houston and R. L. Park, Appl. Phys. Letts. 14, 358 (1969).
14. J. C. Tracy, J. Appl. Phys. 43, 4164 (1972).
15. R. G. Musket and S. W. Taatjes, J. Vac. Sci. Tech. 9, 1041 (1972).
16. R. F. Greene and John Malamas, Phys. Rev. B (in press).
17. R. F. Greene, Thin Solid Films 13, 179-183 (1972).
18. R. F. Greene, Surface Science (Feb. 1973, in press).

19. R. F. Greene and R. W. O'Donnell, Phys. Rev. 147, 599 (1966).

20. R. F. Greene, D. Bixler, and R. N. Lee, J. Vac. Sci. Tech. 8, 75 (1971).

1972 Publications Under This Program

1. R. F. Greene and John Malamas, "Scattering of Carriers in Semiconductors by Screened Surface Charges," Phys. Rev. B (in press).

2. R. F. Greene, "Connection Between the Thermodynamics of Chemisorption on Semiconductor Surfaces and Surface Scattering of Carriers," Thin Solid Films, 13, 179 (1972).

3. R. F. Greene, "The Connection Between the Thermodynamics of Chemisorption on Semiconductor Surfaces and Surface Scattering of Carriers," Surface Science (1972 - in press).

Scattering of Carriers in Semiconductors by Screened Surface Charges

R. F. Greene*
Naval Ordnance Laboratory, White Oak, Maryland 20910
and
John Malamast
Night Vision Laboratory, Fort Belvoir, Virginia 22060

ABSTRACT

A new theory is given of surface scattering in semiconductors by surface point charges, corresponding to trapping in chemisorption bonds or defects. Interference effects, between waves scattered from different scatterers, are evaluated in terms of the statistical structure factor of the surface point charge array. Dielectric image effects are included. The scattering potential is taken from the recent statistical treatment of the three dimensional non-planar semiconductor surface space charge, given by Greene, Bixler, and Lee. The Need for multiple scattering treatment of evanescent states is discussed. Comparison with previous theory is made.

Enclosure (1)
(reference 15)

INTRODUCTION

In 1966 Greene and O'Donnell proposed[1] that the apparent diffuseness of semiconductor surfaces in transport measurements was due to scattering by surface charges, e.g. localized at chemisorbed atoms, defects, etc. They gave a simple calculation of this scattering, finding a rather strong angular dependence. This angular dependence seemed to explain (Greene[2]) the lack of a surface mobility cusp (Greene, Frankl, and Zemel[3]) in the transport measurements of Davis[4] on InSb surfaces. Further confirmation of the GO (Greene-O'Donnell) theory was provided by the measurements of Kamins and MacDonald[5] on the Si-SiO_2 interface. More recent work by Preuss,[6] however, does show evidence of the surface mobility cusp, suggesting that a closer look at surface scattering is needed. Extensive studies of scattering at Si-SiO_2 interfaces have recently been reported (e.g. Sah[7]), also. Motivation for this from another quarter may be cited: Recently it has been shown (Greene[8]) that there exists a general relation between surface scattering rates and the thermodynamics of chemisorption, where the chemisorption bonds provide the trapped charge which causes the scattering.

The GO theory is oversimplified in several respects: a) It neglects the interference terms in the scattering from different surface charges; b) It uses an arbitrary form for the screened potential of the surface charges; and c) It neglects the dielectric image force. The present paper provides a new theory of surface scattering by discrete surface charges which is free of these limitations. We regard the entire screened array of surface charges as a single scatterer. Interference terms can then be treated exactly, in terms of the statistical structure factor of

(1)

the surface charge array. At the same time we replace the arbitrary GO scattering potential by the potential calculated by Greene, Bixler, and Lee,[9] (denoted GBL in this paper) of the inhomogeneous surface space charge region. We also take into account the GBL dielectric image force which, in its screened form, strongly decouples the scattering potential from electrons with small normal momenta. The qualitative features of the GO theory reappear, but with somewhat different angular dependence.

The calculation of scattering by a partially ordered array of scatterers becomes tractable only with use of the statistical properties of the scattering potential. This is also supplied by the GBL theory which treats the semiconductor surface space charge potential as a partially correlated stochastic function of position, determined by the surface distribution of point charges.

The density of surface scatterers is often high enough for scattering interference effects to be very strong. The concept of the differential scattering cross section of individual scatterers then becomes inexact and should be replaced by the dimensionless differential scattering probability of the surface as a whole.

We show that in the Born approximation all interference effects between the scattered and incident waves disappear, for a stochastic scattering potential, but the interferences between different scatterers remain. The need for a multiple scattering treatment is pointed out, particularly for the evanescent or surface currents.

1. Surface Scattering Theory in the Born Approximation

We represent an ideal crystal surface by an infinite potential step at $z = 0$. The unscattered electrons are then described by

$$H^o\psi^o = E\psi^o \quad ; \quad z \geq 0 \quad ; \; H^o = -\hbar^2\nabla^2/2m \tag{1.1a}$$

$$\psi^o = (\sin k_z z)e^{i\vec{K}\cdot\vec{R}} \quad ; \; z \geq 0 \tag{1.1b}$$

$$\psi^o = 0 \quad ; \; z \leq 0 \tag{1.1c}$$

where $E = \hbar^2 k_o^{\,2}/2m$, and $k_o^{\,2} = K^2 + k_z^{\,2}$. (We write 2-dimensional vectors as capitals, e.g. $\vec{K} = (K_x, K_y, 0)$.) Next we introduce a scattering potential $-e\phi(\vec{R},z)$ which produces a scattered wave ψ:

$$(H^o - E - e\phi)(\psi^o + \psi) = 0; \quad z \geq 0 \tag{1.2a}$$

$$\psi = 0 \quad ; \quad z < 0 \tag{1.2b}$$

In the Born approximation

$$(H^o - E)\psi = e\phi\psi^o \quad ; \quad z \geq 0 \tag{1.3}$$

It is convenient to use the 2-dimensional transforms of ϕ and ψ

$$\phi(\vec{Q},z) = \int (d^2R/2\pi)\, \phi(\vec{R},z)e^{-i\vec{Q}\cdot\vec{R}} \tag{1.4a}$$

$$\psi(\vec{Q},z) = \int (d^2R/2\pi)\, \psi(\vec{R},z)e^{-i\vec{Q}\cdot\vec{R}} \tag{1.4b}$$

and to transform Eq. (1.3) to $(\vec{Q},z)$ space

$$(\partial^2/\partial z^2 + \Gamma^2)\psi(\vec{Q},z) = (-2me/\hbar^2)(\sin k_z z)\phi(\vec{Q}-\vec{K},z); \; z \geq 0 \tag{1.5a}$$

where

$$\Gamma = (k_o^{\,2}-Q^2)^{1/2} \text{ for } k_o^{\,2} > Q^2, \text{ and } \Gamma = i(Q^2-k_o^{\,2})^{1/2} \text{ for } k_o^{\,2} < Q^2. \tag{1.5b}$$

The solution of Eq. (1.5a), subject to Eq. (1.2b) can be written

$$\psi(\vec{Q},z) = (-2me/\hbar^2) \int_0^\infty dz'\ G(z;z')\ \phi(\vec{Q}-\vec{K},z')\ \sin k_z z';\ z \geq 0. \quad (1.6a)$$

Here $G(z,z')$ is the one-dimensional Green function

$$G(z,z') = (1/2i\Gamma)\ (\exp i\Gamma\ |z-z'| - \exp i\Gamma|z+z'|\ ) \quad (1.6b)$$

which has the properties

$$G(z,z') = 0 \quad \text{for } z = 0 \quad (1.7a)$$

$$\text{and } (\partial^2/\partial z^2 + \Gamma^2)\ G(z,z') = \delta(z - z') + \delta(z + z'), \quad (1.7b)$$

which ensure that both Eq. (1.2b) and (1.5a) are satisified. The choice of (+) exponents in $G(z,z')$ means that we are requiring that the scattered propagating waves, $Q^2 < k_o^2$, all have the outgoing form $e^{+i\Gamma z}$ for $z \to \infty$, as seems physically reasonable. Moreover, were we to admit incoming scattered waves, these would produce divergent exponential solutions for $Q^2 > k_o^2$.

The GBL potential produced by surface point charges consists of a planar or band-bending term ϕ_p which depends on z only, and an inhomogeneity term, $\phi(\vec{R},z)$, which produces scattering and has the form

$$\phi(\vec{Q},z) = \phi(\vec{Q},0)\ e^{-\kappa z}, \quad (1.8a)$$

$$\text{where} \qquad \kappa = (q_s^2 + Q^2)^{1/2}, \quad (1.8b)$$

and where q_s is the effective inverse screening length near the surface:

$$q_s^2 = (4\pi e^2 n_B/\varepsilon_+ kT)\ \exp(e\phi_{ps}/kT) \equiv q_o^2\ (\exp e\phi_{ps}/kT) \quad (1.8c)$$

Here n_B is the bulk electron concentration and ϕ_{ps} is the value of the band-bending potential at the surface. It might be objected that the use of the Fermi-Thomas approximation in GBL theory is inconsistent with our scattering model, viz. Eqs. (1.1c) and (1.2b), whereby carrier wave functions are terminated at the surface. It has been shown (Greene[10]) that the screening approximations are negligable for surface fields below about 5×10^4 V/cm in non-degenerate semiconductors. If we use the simple z-dependence of Eq. (1.8a), then we can write the scattered solution Eq. (1.6a) in the explicit form

$$\psi(\vec{Q},z) = (me/2\hbar^2)\ \phi(\vec{Q}-\vec{K},0)\ (F_p\ e^{i\Gamma z} + F_s(z)), \tag{1.9a}$$

where $$F_p = F_p^* = 8\kappa k_z/((\kappa^2 + \Gamma^2 + k_z^2)^2 - 4k_z^2\Gamma^2), \tag{1.9b}$$

and $$F_s = F_s^* = 2i\left[e^{i(k_z-\kappa)z}/(\kappa^2-k_z^2 + \Gamma^2 - 2i\kappa k_z) + c.c.\right]. \tag{1.9c}$$

Here $$\kappa = \kappa(\vec{Q}-\vec{K}) = ((\vec{Q}-\vec{K})^2 + q_s^2)^{1/2} \tag{1.9d}$$

and Γ is given by Eq. (1.5b). The F_p term is a propagating wave for $Q^2 < k_o^2$, but is evanescent for $Q^2 > k_o^2$. The F_s term is evanescent for all values of $\vec{Q}$. Electrons scattered into evanescent states clearly interact strongly with the scattering potential ϕ and will be multiple-scattered. A treatment of these states will be given elsewhere.

2. Scattered Flux Density from a Partially Random Scatterer

We now calculate the scattered flux density $\vec{J}$, and then afterwards introduce the statistical or random properties of the scattering potential. The probability flux density for a state $\psi = \psi^o + \psi$, viz

$$\vec{J} = (i\hbar/2m)\ (\Psi\nabla\Psi^* - c.c.), \tag{2.1}$$

has three distinct terms

$$\vec{J} = \vec{J}(\psi^o;\ \psi^o) + \vec{J}(\psi;\psi) + \vec{J}(\psi^o;\psi) \tag{2.2}$$

corresponding to the unscattered wave, the scattered wave, and the interference between the scattered and unscattered waves, respectively. These take on complicated forms when the scattering potential has the complicated form of the inhomogeneous space charge potential $\phi(\vec{R},z)$.

Simplifications occur, however, when we make use of the statistical properties of the scattering potential. For our purposes $\phi(\vec{R},z)$ may be treated as a random function of $\vec{R}$ with two basic ensemble average properties:

$$\{\phi(\vec{R},z)\} = 0\ , \tag{2.3a}$$

and $$\{\phi(\vec{R},z)\ \phi(\vec{R}+\Delta\vec{R},z) = \text{function of } \Delta\vec{R} \text{ and } z \text{ but not of } \vec{R}. \tag{2.3b}$$

Eq. (2.3a) indicates that we have subtracted out the mean value of the space charge potential, as mentioned above in connection with Eq. (1.8a). Eq. (2.3b) means that the various probability density functions for $\phi(\vec{R})$ are uniform in $\vec{R}$. Because of this statistical uniformity, we may equate ensemble averages with spatial averages, e.g.

$$\{\phi(\vec{R})\} = \bar{\phi} = \lim_{L\to\infty} L^{-2} \int_{L_2} d^2R\, \phi(\vec{R}) \tag{2.4}$$

For use in our scattering theory it is convenient to re-express conditions (2.3a) and 2.3b) in $\vec{Q}$-space. This is possible because each member of the statistical ensemble of functions $\phi(\vec{R},z)$ can be represented just as well by its Fourier transform $\phi(\vec{Q},z)$. Equations (2.3a) and (2.3b) then appear as

$$\{\phi(\vec{Q},z)\} = 0 \tag{2.5a}$$

and
$$\{\phi(\vec{Q},z)\phi(\vec{Q}',z)^*\} = 4\pi^2\, \delta(\vec{Q} - \vec{Q}')\, g_\phi(\vec{Q},z), \tag{2.5b}$$

where $g_\phi(\vec{Q})$ is the spectral density of $\phi(\vec{R},z)$:

$$g_\phi(\vec{Q},z) = \lim_{L\to\infty} L^{-2}|\phi_L(\vec{Q},z)|^2 \qquad \text{and } \phi_L \equiv 0 \text{ for } R^2 > L^2 \tag{2.5c}$$

(2.5a) follows directly from ensemble-averaging Eq. (1.4a) and using Eq. (2.3a). Eq. (2.5b) can be obtained by writing

$$\{\phi(\vec{Q})\ \phi(\vec{Q}')^*\} = \int (d^2R/2\pi) \int (d^2R'/2\pi)\ \{\phi(\vec{R})\phi(\vec{R}')\}\ \exp(i\vec{Q}\cdot\vec{R} - i\vec{Q}'\cdot\vec{R}')$$

and then imposing the statistical uniformity condition (2.3b), giving

$$\{\phi(\vec{Q})\phi(\vec{Q}')^*\} = \delta(\vec{Q} - \vec{Q}') \int (d^2\Delta R/2\pi)\ \rho_\phi(\Delta\vec{R})\ \exp - i\vec{Q}\cdot\Delta\vec{R}.$$

where $\rho_\phi(\Delta\vec{R}) = \lim_{L\to\infty} L^{-2} \int d^2R\ \phi_L(\vec{R},z)\ \phi_L(\vec{R}+\Delta\vec{R},z)$

Eq. (2.5b) then follows by means of the Wiener-Khinchine relation, (Ming Chen Wang and Uhlenbeck[11]).

We can now use Eqs. (2.5a) and (2.5b), the statistical properties of the space charge potential, to simplify the probability flux density $\vec{J}$, when the latter is ensemble-averaged. First we note that in the Born approximation ψ is a linear functional of ϕ, so that

(1).

$$\{\vec{J}(\psi^o,\psi)\} = 0 \ . \qquad (2.6)$$

Particle flux conservation in surface scattering requires that $\{J_z(\psi_o+\psi,\ \psi_o+\psi)\}$ vanish exactly, since carriers are assumed neither to go through the surface nor to be created there. Of course $J_z(\psi_o,\ \psi_o) = 0$ because ψ_o is a standing wave. Furthermore, the exact ψ contains only outgoing ($k_z > 0$) waves for $z \to \infty$ so that $\{J_z(\psi,\psi)\} > 0$. Therefore the exact interference terms $\{J_z(\psi,\psi_o)\}$ + c.c. must be negative. Eq. (2.6) then means that our approximate ψ fails to conserve particle flux: this will be discussed elsewhere. Next, we point out the great simplification produced by Eq. (2.5b) in the scattered flux density $\vec{J}(\psi,\psi)$ whereby

$$\vec{J}(\psi,\psi) = (i\hbar/2m)(me/2h)^2 \int (d^2Q/2\pi) \int (d^2Q'/2\pi)\phi(\vec{Q}-\vec{K},0)\phi(\vec{Q}'-\vec{K},0)^*$$

$$[((F_p e^{i\Gamma z}+F_s)e^{i\vec{Q}\cdot\vec{R}})\nabla((F_p' e^{-i\Gamma^* z}+F_s')e^{-i\vec{Q}'\cdot\vec{R}})-c.c.] \qquad (2.7)$$

is reduced to an expression which, as shall show below, has a simple semi-classical interpretation and is capable of complete evaluation:

$$\{\vec{J}(\psi,\psi)\} = (me^2/8h^2) \int d^2Q\ g_\phi(Q-K,0)[(2Q+1_z(\Gamma+\Gamma^*))F_p^2 \exp(i\Gamma z - i\Gamma^* z)$$

$$+ 2\vec{Q}\ F_s^2 + 2\vec{Q}F_pF_s(e^{i\Gamma z}+c.c) - \vec{1}_z\ F_p\hat{F}_s e^{-\kappa z}] \qquad (2.8a)$$

where

$$-\hat{F}_s = [(\kappa-ik_z)(e^{i\Gamma z}-c.c) + i(e^{i\Gamma z}-c.c)]M\ e^{ik_z z}-c.c \qquad (2.8b)$$

and

$$M = 2i((\kappa-ik_z)^2 + \Gamma^2)^{-1}, \text{ and } \vec{1}_z = (0,0,1) \qquad (2.8c)$$

The F_p term is propagating for $Q^2 < k_o^2$, evanescent for $Q^2 > k_o^2$. The F_s and $\hat{F}_s$ terms are evanescent for all values of $\vec{Q}$. These evanescent fluxes, corresponding to real surface currents, are not correctly given in the Born approximation because the re-scattering of electrons in such states cannot be neglected in any approximation. In this paper we will therefore treat only the propagating flux density

$$\{\vec{J}\}_p = (me^2/4\hbar^3) \int_{Q^2<k_o^2} d^2Q \; F_p^2 \; g_\phi(\vec{Q}-\vec{K},0)(Q_x, Q_y, \Gamma). \tag{2.9}$$

This takes on a clear semi-classical form in terms of the angular coordinates of the scattered waves

$$Q_x = k_o \sin\theta \cos\eta \,, \quad Q_y = k_o \sin\theta \sin\eta \,. \tag{2.10a}$$

$$\text{Writing } d^2Q = Q\, dQ\, d\eta = -k_o^2\, \mu d\mu\, d\eta, \; (\mu = \cos\theta) \,, \tag{2.10b}$$

one gets

$$\{\vec{J}\}_p = \int_0^1 d\mu \int_0^{2\pi} d\eta \; f(\vec{K},-k_z;\mu,\eta)\vec{v} \tag{2.11a}$$

where

$$\vec{v} = (\hbar/m)(Q_x, Q_y, \Gamma) \tag{2.11c}$$

is the scattered velocity vector, and

$$f(\vec{K},-k_z;\mu,\eta) = (me/2\hbar^2)^2 \mu k_o^2 \; F_p^2 \; g_\phi(\vec{Q}-\vec{K},0) \tag{2.11c}$$

is the scattered distribution function, the number of classical electrons per unit solid angle at (μ,η).

Although it has a clear semi-classical interpretation, Eq. (2.11a) is somewhat more complicated than the corresponding expression in the theory of scattering from a finite range potential (Schiff[12]).

There, only one propagation vector is seen at a distant detector because the scatterer subtends only an infinitesimal solid angle at the detector. The range (2π) of scattering angles appears in Eq. (2.11a) because the scattering surface subtends the solid angle (2π) at a detector, no matter how far from the surface it may be.

3. Differential Scattering Probability

The concept of differential scattering cross section, appropriate for finite range scatterers, is generally not useful for surface scattering except when the surface density of scatterers is low enough to ignore interference effects and screening interactions. The generally appropriate concept is that of the dimensionless differential surface scattering probability $w(\vec{K},-k_z;\mu,\eta)$ which we define as

$$w(\vec{K},-k_z;\mu,\eta) = N(\mu,\eta)/N_o(\vec{K},-k_z) \tag{3.1}$$

where $N_o(\vec{K},-k_z)$ is the number/sec. of electrons incident on unit area of the surface with momentum $(K_x, K_y, -k_z)$, and $N(\mu,\eta)d\mu d\eta$ is the number/sec. of particles scattered into solid angle $d\mu d\eta$ from unit area of the surface.

Equation (2.11a) enables us to find $N(\mu,\eta)$ directly. Evidently

$$N(\mu,\eta) = \mu\, v\, f(\mu,\eta). \tag{3.2}$$

On the other hand, the unperturbed wave function ψ^o of Eq. (1.1b) describes an incident flux density of magnitude $v/4$, so that

$$N_o(\vec{K},-k_z) = \mu_{\vec{K}} v/4, \quad \text{where} \quad \mu_{\vec{K}} = -k_z/k_o < 0 . \tag{3.3}$$

We thus obtain

$$w(\vec{K},-k_z;\mu,\eta) = (-\mu/\mu_{\vec{K}})f(\mu,\eta) = (-\mu^2/\mu_{\vec{K}})(mek_o/\hbar^2)^2 F_p^2\, g_\phi(\vec{Q}-\vec{K},0), \tag{3.4}$$

where F_p is given by Eq. (1.9b) and $g_\phi(\vec{Q}-\vec{K},0)$ is the spectral density of the scattering potential for the surface momentum change $(\vec{Q} - \vec{K})$.

This spectral density $g_\phi(\vec{Q},z)$ is expressed in the GBL theory in terms of the spectral density $g_{\delta\Omega}(\vec{Q})$ of the surface charge density Ω, or rather of $\delta\Omega = \Omega(\vec{R}) - \bar{\Omega}$ (by means of Poisson's equation, the static electron response function, and the Maxwell boundary conditions)

$$g_\phi(\vec{Q},z) = \mathcal{R}(\vec{Q})^2\, e^{-2\kappa z}\, g_{\delta\Omega}(\vec{Q}) \tag{3.5a}$$

where

$$\mathcal{R}(\vec{Q}) = (4\pi/\varepsilon_+)^2(\kappa + \gamma Q)^{-2},\ (\gamma = \varepsilon_-/\varepsilon_+ < 1) \tag{3.5b}$$

describes the response of the semiconductor surface space charge region to an arbitrary surface charge distribution. Suppose, in particular, that $\Omega(\vec{R})$ consists of an array of point charges, e.g. associated with chemisorption bonds, occupying some of the sites $\vec{A}$ of a regular surface lattice (mesh). In that case $g_{\delta\Omega}$ is essentially the statistical structure factor $S(\vec{Q})$ of that array:

$$g_{\delta\Omega}(\vec{Q}) = (a\,\bar{\Omega}^2/4\pi^2)\, S(\vec{Q}) \tag{3.6a}$$

$$S(\vec{Q}) = \sum_{\Delta\vec{A}} (p(\Delta\vec{A})/\bar{n} - 1)e^{i\vec{Q}\cdot\Delta\vec{A}} + \sum_{\vec{Q}_i \neq 0} \delta(\vec{Q}-\vec{Q}_i)(4\pi^2/a) \tag{3.6b}$$

Here $n(\vec{A}) = 0,1$ is the occupation number of site $\vec{A}$, $\bar{n}$ is the mean of $n(\vec{A})$,

$$\bar{n} = \{n\} = a\bar{\Omega}\ , \tag{3.6c}$$

where a is the unit mesh area. Also, $p(\Delta\vec{A})$ is the pair correlation function

$$p(\Delta\vec{A}) = \{n(\vec{A})n(\vec{A}+\Delta\vec{A})\} / \bar{n} \; ; \quad p(0) \equiv 1 \; . \tag{3.6d,e}$$

and $\vec{Q}_i$ are the reciprocal mesh vectors

$$\vec{Q}_i \cdot \vec{A} = 2\pi \text{ integer, or zero.} \tag{3.6f}$$

These reciprocal mesh vectors determine the features of the evanescent states but do not directly appear in the propagating flux $\{\vec{J}\}_p$, and so can be omitted in this paper. We thus obtain the explicit form of the differential surface scattering probability

$$w(\mu,n) = w_{GO}(\mu,n) \left(\frac{2\kappa}{\kappa + \gamma |\vec{Q} - \vec{R}|}\right)^2 \bar{n} \, S(\vec{Q}-\vec{K}) \tag{3.7a}$$

where

$$w_{GO} = \frac{\bar{n}a}{-\mu_{\vec{K}}} \left(\frac{4\Gamma k_z}{(\kappa^2+k^2+\Gamma^2)^2 - 4k_z^2\Gamma^2}\right)^2 \left(\frac{2me^2}{\hbar^2\varepsilon_+}\right)^2 \tag{3.7b}$$

is the corresponding result of the GO calculation. The factors multiplying w_{GO} express the effect of taking into account properly the screening potential and the interference of waves scattered from different scatterers.

The simplest interference situation to analyze is, of course, that of no correlation at all in the occupation numbers: If

$$p(\Delta\vec{A}) = \bar{n} \quad \text{for all } \Delta\vec{A} \neq 0 \tag{3.8a}$$

then

$$S^o(\vec{Q}) = S^o(0) = (1 - \bar{n})/\bar{n} \; . \tag{3.8b}$$

Then if $\bar{n} << 1$, w is linear in $\bar{n}$ and an effective surface scattering cross section might be introduced. Next consider the effect of a short range correlation: If

$$p(\Delta\vec{A}) = \bar{n} \quad \text{for all} \quad |\Delta\vec{A}|k_o \gtrsim 1/10 \tag{3.9a}$$

then

$$S(\vec{Q}) = S(0) = \sum_{\Delta A} (p(\Delta\vec{A})/\bar{n} - 1) \quad . \tag{3.9b}$$

In both of these cases the scattering is determined by S(0) which, as has been shown elsewhere (Greene[8]) is a thermodynamic property of the chemisorbed charged adatoms, if these have reached equilibrium. If the distribution has not reached equilibrium, so that S(0) cannot be obtained from statistical thermodynamic arguments, some guidance in the choice of $p(\Delta\vec{A})$ is available from the sum rule

$$\int_{BZ} d^2Q \;\; S(\vec{Q}) = (4\pi^2/\bar{n}\, a)(1 - \bar{n}) \tag{3.10}$$

in which the integral goes over one Brillouin zone of the reciprocal mesh, and which arises from Eq. (3.6e).

Finally, we consider the space charge form factor,

$$B = 4\kappa^2 \, (\kappa + \gamma|Q - K|)^{-2}, \tag{3.11}$$

appearing in Eq. (3.7a), which corrects for the arbitrary potential used in the GO treatment, viz $(e/\varepsilon_+ r)\exp(-q_o r)$, for $z \geq 0$. For small angle scattering events one can see that

$$B = 4, \quad \text{for} \quad |Q - K| << q_s \tag{3.12}$$

Thus the Fourier coefficients of the Yukawa potential mentioned above are exactly half the correct ones, for $\vec{Q} \to 0$. At the other extreme, one can consider large angle scattering for $q_s^2/k_o^2 << 1$, in which case

$$B = 4(1 + \gamma)^{-2} \quad \text{for } |\vec{Q} - \vec{K}| >> q_s. \tag{3.13}$$

This simply means that large angle scattering events are determined by the unscreened Coulomb singularity itself, which has the form $(e/\varepsilon_+ r)(2/(1 + \gamma))$.

4. Dielectric Image Effects

The polarization energy of an electron changes as the electron is brought nearer the interface between two dielectrics. This can be expressed (Abraham and Becker[13]) in terms of a dielectric image force, and has already entered the scattering potential ϕ directly, as is shown by the factor $\gamma = \varepsilon_-/\varepsilon_+$ in the spectral density g_ϕ in Eq. (3.5b).

But there is also a direct dielectric image repulsion of each electron from the surface when $\gamma < 1$. In GBL it was shown that for semiconductors the work done on an electron in bringing it and its screening cloud closer to a surface can be expressed in terms of a screened image potential ϕ_I given by

$$-e\phi_I = (b\, e^2/4\varepsilon_+ z) \exp -q_s z \ , \tag{4.1}$$

where b is a constant; between unity and $(\gamma - 1)/(\gamma + 1)$. Being independent of R, this is not a scattering potential. Nevertheless, the scattering is weakened because ϕ_I decreases the amplitude of the unscattered wave functions ψ^o near the surface.

This direct dielectric image repulsion can be introduced into the foregoing scattering theory very simply, albeit crudely, by terminating ψ_o at the classical turning point z_I instead of at the surface $z = 0$, z_I being given by

$$-e\phi_I(z_I) = \hbar^2 k_z^2/2m \quad (z_I > 0) \ . \tag{4.2}$$

Electrons incident at grazing angles have small k_z and hence have large values of z_I and are strongly de-coupled from the scattering potential. We thus replace Eq. (1.1) by

$$\psi^o = (\sin k_z(z - z_I))e^{i\vec{K}\cdot\vec{R}}, \quad z \geq z_I \tag{4.3a}$$

$$\psi^o = 0, \qquad z < z_I. \tag{4.3b}$$

For the Born approximation treatment of Section (1) to remain valid, we must correspondingly replace Eq. (1.2b) by

$$\psi = 0, \qquad z \leq z_I \ . \tag{4.4}$$

The Born approximation Eq. (1.5a) is then replace by

$$(\partial^2/\partial z^2 + \Gamma^2)\psi(\vec{Q},z) = (-2me/\hbar^2)\sin k_z(z-z_I)\phi(\vec{Q}-\vec{K},z), \ z \geq z_I. \tag{4.5}$$

The scattered wave Eq. (1.6a) is now replaced by

$$\psi(\vec{Q},z) = (-2me/\hbar^2)\int_{z_I}^{\infty} dz' \ G_D(z,z')\phi(\vec{Q}-\vec{K},z')\sin k_z(z'-z_I) \tag{4.6}$$

where now the <u>displaced</u> Green function

$$G_D(z,z') = (1/2i\Gamma)(\exp i\Gamma|(z-z_I)-(z'-z_I)| - \exp i\Gamma|(z-z_I) + (z-z_I)|) \tag{4.7a}$$

has the property

$$G_D(z,z') = 0 \text{ for } z = z_I \tag{4.7b}$$

(which ensures that Eq. (4.4) is satisfied), and the property

$$(\partial^2/\partial z^2 + \Gamma^2)G_D(z,z') = \delta(z-z') + \delta(z+z'-2z_I) \tag{4.7c}$$

(which ensures that Eq. (4.5) is satisfied.) Here the fact that

$$\phi(\vec{Q}-\vec{K},z') = \phi(\vec{Q}-\vec{K},0)\ \exp(-\kappa z') = \phi(\vec{Q}-\vec{K},\Delta z)\ \exp(-\kappa z_I), \qquad (4.8)$$

where $\Delta z' = z' - z_I$, allows Eq. (4.6) to be written as

$$\psi(\vec{Q},z) = (\exp-\kappa z_I)(2me/\hbar^2)\int_0^\infty d\Delta z'\ G(\Delta z,\Delta z')\sin(k_z\Delta z')\phi(\vec{Q}-\vec{K},\Delta z') \qquad (4.9)$$

where now $G(\Delta z,\Delta z')$ has exactly the same functional form as the Green function used in Eq. (1.6a) for the scattered wave without this dielectric image effect. Thus the entire effect of shifting the unscattered wave ψ^o a distance $z_I(k_z)$ is merely to shift all the scattered waves by the same amount and to change their amplitudes by exp $(-\kappa z_I)$.

Because this factor is independent of $\vec{R}$ and z, the scattered current density is unchanged except for the appearance of a multiplicative factor $\exp(-2\kappa z_I)$. Thus for electrons the differential surface scattering probability of Eq. (3.7a) becomes

$$w(\mu,\eta) = w_{GO}(\mu,\eta)\quad B\ (\exp\ -2\kappa z_I)\bar{n}\ S(\vec{Q}-\vec{K}) \qquad (4.10)$$

where B, the space charge form factor, is given by Eq. (3.11). Here $\cos^{-1}\mu$ and η are the angles of the emerging electron in spherical coordinates.

As noted above, the dielectric image factor $(\exp-2\kappa z_I(k_z))$ strongly decreases the scattering rate for electrons at grazing incidence, because z_I increases as k_z decreases. Inasmuch as $\kappa = (q_s^2 + (\vec{Q}-\vec{K})^2)^{1/2}$, it is clear that this suppression of scattering occurs mostly for large angle scattering. This is indeed plausible, since the spatial shift of the unscattered wave primarily cuts down the overlap of ψ^o with the more singular part of the scattering potential.

5. Fuchs Reflectivity; Conclusions

We use the general boundary condition formalism (Greene[14]) to get the Fuchs reflectivity p and kinetic specularity W_o from the differential scattering probability of Eq. (4.10): For an isotropic surface

$$W_o(\mu_+) = 1 - \int_{-1}^{0} d\mu_- \int_{0}^{2\pi} d\Delta\eta(-\mu_-/\mu_+) w_s(\mu_-,\eta_-|\mu_+,\eta_+) \tag{5.1a}$$

$$p(\mu_+) = 1 - \int_{-1}^{0} d\mu_- \int_{0}^{2\pi} d\Delta\eta(-\mu_-/\mu_+) w_s(\mu_-,\eta_-|\mu_+,\eta_+)\left[1 - \cos\Delta\eta\left(\frac{1-\mu_-^2}{1-\mu_+^2}\right)^{1/2}\right]. \tag{5.1b}$$

where $\cos^{-1}\mu_+$ is the angle between the scattered k-vector and the inward normal to the surface, and $\Delta\eta = \eta_- - \eta_+$ is the angle between surface components of scattered and incident k-vectors.

These integrations, which could be carried out analytically in the simpler GO theory, unfortunately had to be carried out numerically for w_s given by Eq. (4.10). We carried out the integrations for the completely uncorrelated ("pure random") distribution of surface charges, for which the structure factor (leaving out the Bragg terms outside the Brillouin zone) is

$$S^o(\vec{Q}) \doteq S^o(0) = (1 - \bar{n})/\bar{n} \quad , \text{(for } p(\Delta\vec{A}) = \bar{n} \text{ for } \Delta\vec{A} \neq 0) \tag{5.2a}$$

in which case Eq. (4.10) reduces to the simpler form

$$w_s = w_{GO}\, B(\exp - 2\kappa z_I)(1 - \bar{n}) \tag{5.2b}$$

in which case $1 - W_o$ and $1 - p$ are linear in $\bar{n}$ for $\bar{n} << 1$.

The scatterers are charged so that an uncorrelated distribution is not really to be expected except when $\bar{n}$ is close to zero. Correlation effects can depress $S(\vec{Q})$ and w_s very significantly, as we now show for the case of depressed nearest neighbor occupation $p(1) < \bar{n}$ of a simple square mesh. From Eq. (3.6b)

$$S(\vec{Q}) = (1 - \bar{n} - 2(\bar{n}-p(1))(\cos Q_x A_o + \cos Q_y A_o))/\bar{n} \geq 0. \qquad (5.3)$$

In the absence of a statistical thermodynamic calculation of $p(1)$, we might guess a form (which keeps $S(\vec{Q})$ positive definite).

$$\bar{n} = p(1) = (1/4)(1-\bar{n})(1-e^{-\alpha}) \qquad (5.4a)$$

where

$$\alpha = 2e^2/A_o(\varepsilon_+ + \varepsilon_-)kT \qquad (5.4b)$$

is, roughly, the nearest neighbor Coulomb energy in units of kT. Since in w_s only small values of Q_x, $Q_y \sim k_o << |A_o|^{-1}$ occur, we can set

$$S(\vec{Q}) = S(0) = (1 - \bar{n})e^{-\alpha}/\bar{n} = S^o(0)e^{-\alpha} \qquad (5.5)$$

so that our calculated (uncorrelated) values of $1 - W_s$ and $1 - p$ have to be multiplied by the very strong factor $e^{-\alpha}$.

The calculations have been carried out for spherical energy surfaces and so are most directly applicable to semiconductors like InSb (Willardson[15]) whose electron effective mass, $0.013m_o$, and dielectric constant, $\varepsilon_+ = 17$, were used. Numerical results for p and W_o versus the emergence angle cosine μ_+ are plotted in Figures 1 through 4 for three different forms of differential scattering probability w_s. Curves labelled GME correspond to the use of

Eq. (4.10). Curves labelled GM correspond to the use of Eq. (4.10) with the dielectric image factor (exp $-2\kappa z_I$) omitted, i.e. to Eq. (3.7a). Curves labelled GO correspond to the GO theory,[1] i.e. to the use of w_{GO} of Eq. (3.7b). In Fig. 5 we show the specific effect of the dielectric image factor, expressed as

$$\{\exp - 2\kappa z_I\} \equiv (1 - p_{GME})/(1 - p_{GM}), \qquad (5.6)$$

plotted as a function of the emergent angle cosine. The dielectric image factor is more effective for slower particles and nearer grazing emergence because, in both cases, k_z is smaller.

The qualitative features of the simpler GO theory are retained: a), $p \to 1$ for grazing emergence; and b), the Fuchs diffusivity $(1 - p)$ is much smaller than the total scattering probability $(1 - W_0)$. But the use of a realistic treatment of the screening of the surface scattering potential has increased its Fourier transform and hence $(1 - p)$ by about a factor of four. This is partially compensated by the dielectric image effect, which decreases the Fuchs diffusivity $(1 - p)$, particularly at grazing angles. For such angles k_z is small, z_I is large and (exp $- 2\kappa z_I$) becomes much less than unity.

Compared with the GO theory, as Figures 1 thru 4 show, the present theory gives a weakened angular dependence of p at grazing angles. This makes cuspid behavior in the surface mobility somewhat more understandable.

One unwelcome feature of the GO theory which is retained in the present theory is the breakdown for larger values of $\bar{n}$, where p can become negative. We can now see, however, that this breakdown is not due to the neglect of interference effects but has to be ascribed to the use of the Born approximation with

its neglect of multiple scattering. This is particularly serious for evanescent states, a treatment of which will be given elsewhere.

A Boltzmann transport calculation of surface mobility using the calculated values of the Fuchs p now becomes possible and is being carried out. That will then permit the scattering model of the present calculation to be tested against surface mobility measurements, e.g. those of Preuss[6] on InSb, those of Sah[7] on the Si:SiO_2 interface, etc. It should also be possible to test the present surface scattering theory, or rather the surface charge structure factor deduced from a fit to transport data, against structure factor information from chemisorption isotherm data, using the new surface scattering-chemisorption relation of one of us (Greene[8]). Such experiments, involving chemisorption and electrical transport studies in thin single crystal films of IV-VI semiconductors with exposure to oxygen, hydrogen, etc. are being carried out at Naval Ordnance Laboratory (Lee[16]). Further scattering calculations are also being pursued replacing the Born approximation by a one-particle Green function method which conserves particle flux exactly, and which includes ellipsoidal energy surface effects.

FIGURE CAPTIONS

Fig. 1a: p versus μ_+; $\bar{n}/a = 10^9$ cm^{-2}, $\hbar^2k^2/2m^* = 0.026$ eV. $m^*/m = 0.013$, $\varepsilon_+ = 17$, $q_o = 1.33 \times 10^5$ cm^{-1}.

Fig. 1b: W_o versus μ_+; $\bar{n}/a = 10^9$ cm^{-2}, $\hbar^2k^2/2m^* = 0.026$ eV, $m^*/m = 0.013$, $\varepsilon_+ = 17$, $q_o = 1.33 \times 10^5$ cm^{-1}.

Fig. 2: p and W_o versus μ_+; $\bar{n}/a = 10^9$ cm^{-2}, $\hbar^2k^2/2m^* = 0.026$ eV, $m^*/m = 0.013$, $\varepsilon_+ = 17$, $q_o = 1.33 \times 10^6$ cm^{-1}.

Fig. 3: p versus μ_+; $\bar{n}/a = 10^9$ cm^{-2}, $\hbar^2k^2/2m^* = 0.26$ eV, $m^*/m = 0.013$, $\varepsilon_+ = 17$, $q_o = 1.33 \times 10^5$ cm^{-1}.

Fig. 4: p versus μ_+; $\bar{n}/a = 10^9$ cm^{-2}, $\hbar^2k^2/2m^* = 0.0026$ eV, $m^*/m = 0.013$, $\varepsilon_+ = 17$, $q_o = 1.33 \times 10^5$ cm^{-1}.

Fig. 5: $\{\exp - 2\kappa z_I\}$ versus μ_+ for different values of $\hbar^2k^2/2m^*$, $m^*/m = 0.013$, $\varepsilon_+ = 17$, $q_o = 1.33 \times 10^5$ cm^{-1}.

REFERENCES

*Supported by Advanced Research Projects Agency, Department of Defense.

†Parts of this work were submitted to the University of Maryland in partial fulfillment of the requirements for the M.S. degree in Physics.

1. R. F. Greene and R. W. O'Donnell, Phys. Rev. 147, 599 (1966).
2. R. F. Greene, Phys. Rev. 141, 609 (1966).
3. R. F. Greene, D. R. Frankl, and J. N. Zemel, Phys. Rev. 118, 967 (1960); R. F. Greene, Phys. Rev. 131, 592 (1966).
4. J. L. Davis, Surface Science 2, 33 (1964).
5. T. I. Kamins and N. C. MacDonald, Phys. Rev. 167, 754 (1968).
6. E. Preuss, Phys. Rev. B1, 3392 (1970).
7. C. T. Sah, T. H. Ning, and L. L. Tschopp, Surface Science 30, 131 (1972).
8. R. F. Greene, Proceedings 1972 International Conference on Thin Films, Venice, Italy, May 18, 1972, (Thin Solid Films 13, 179 (1972).
9. R. F. Greene, D. R. Bixler, and R. N. Lee, J. Vac. Sci. Tech. 8, 75 (1971).
10. R. F. Greene, Surface Science 2, 101-113 (1964).
11. Ming Chen Wang and G. E. Uhlenbeck, Rev. Mod. Phys. 17, 327 (1945).
12. L. I. Schiff, "Quantum Mechanics," McGraw-Hill Book Co. (N.Y. 1955).
13. M. Abraham and R. Becker, "Theory of Electricity," Blackie & Son, London, (1937).
14. R. F. Greene, Phys. Rev. 141, 687 (1966).
15. R. K. Willardson and A. C. Beer, editors, "Semiconductors and Metals, Vol. 1, Physics of III-V Compounds."

16. R. N. Lee, private communication (1972).

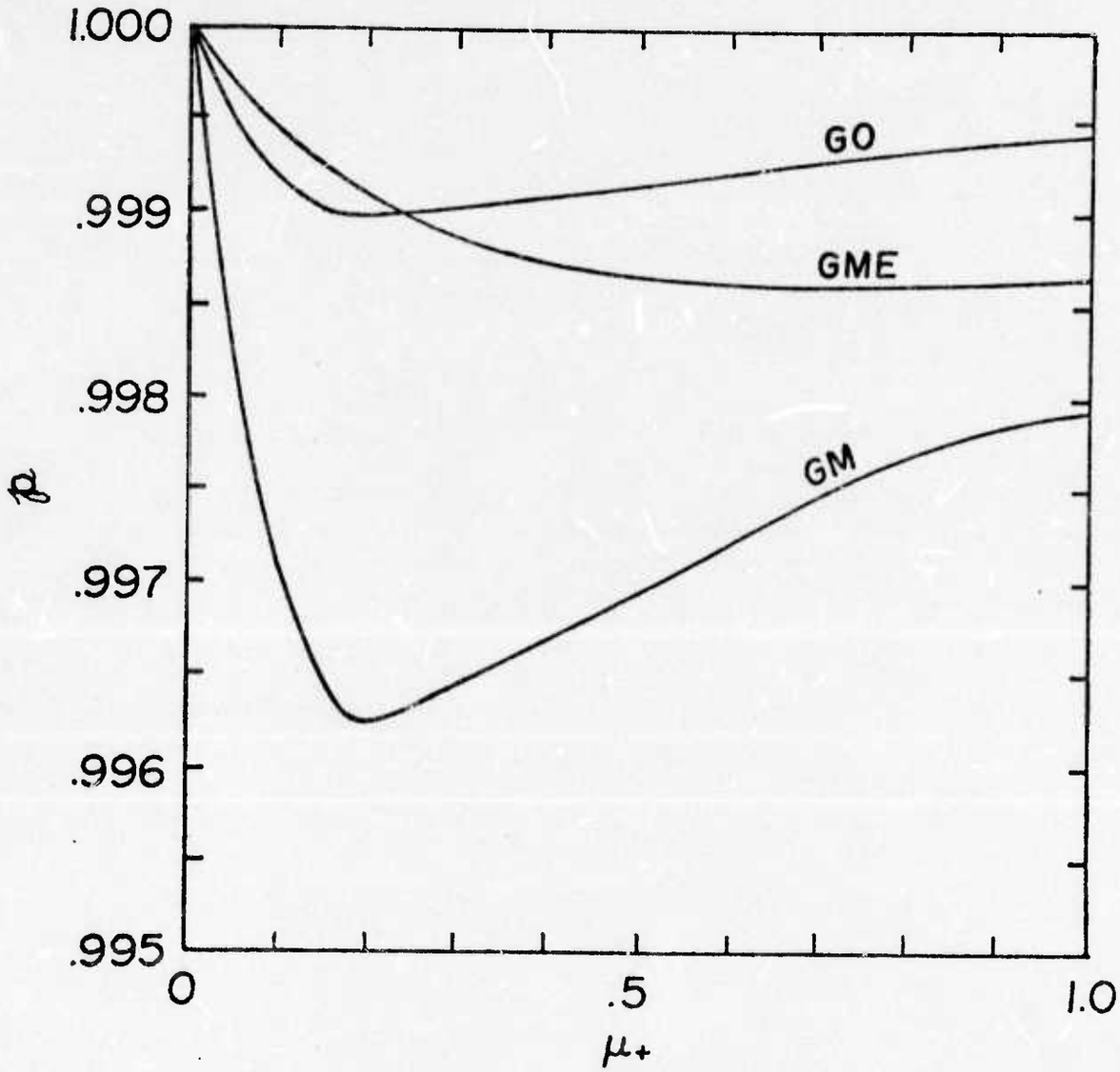

ENCLOSURE (1)

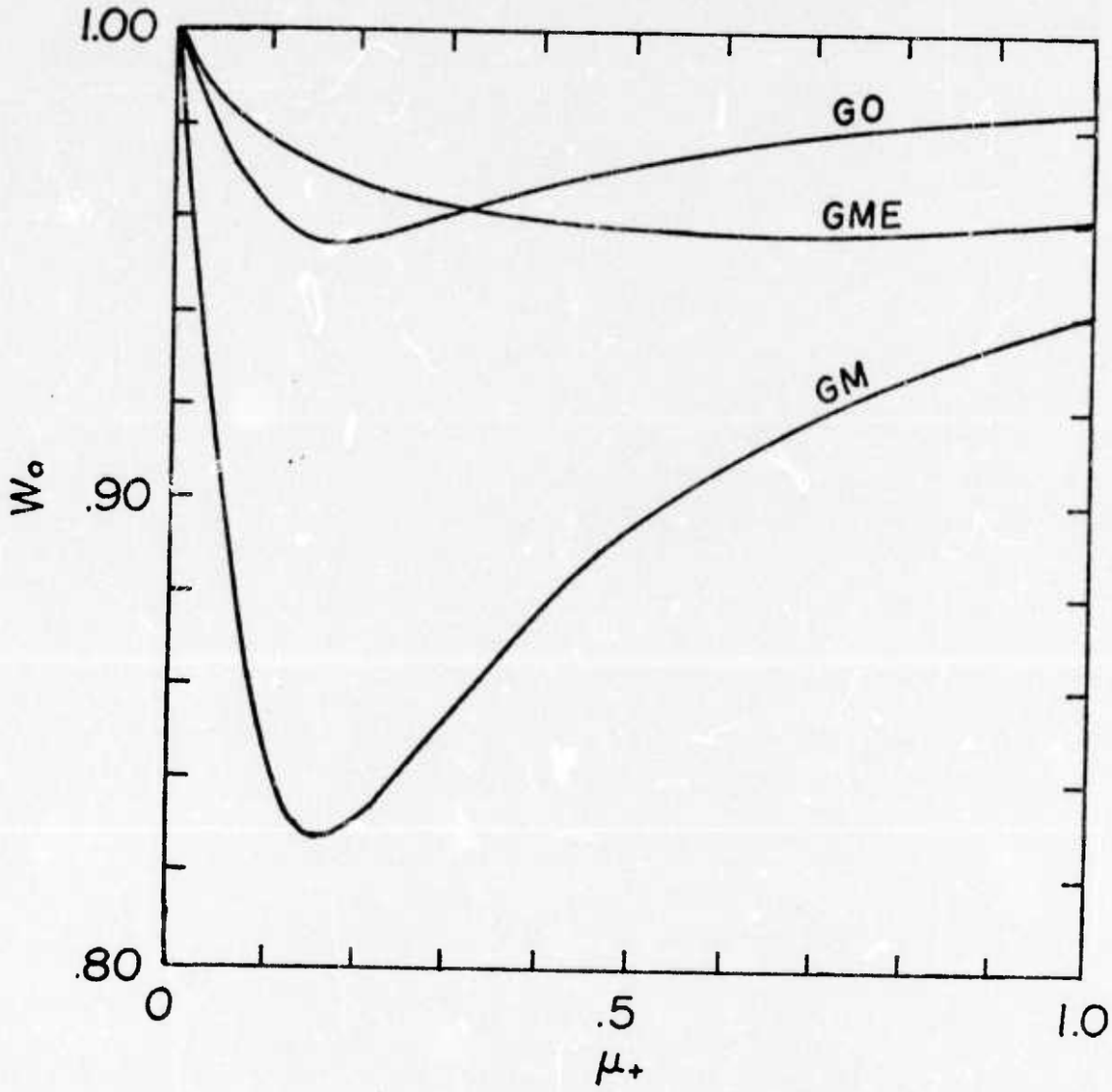

ENCLOSURE (1).

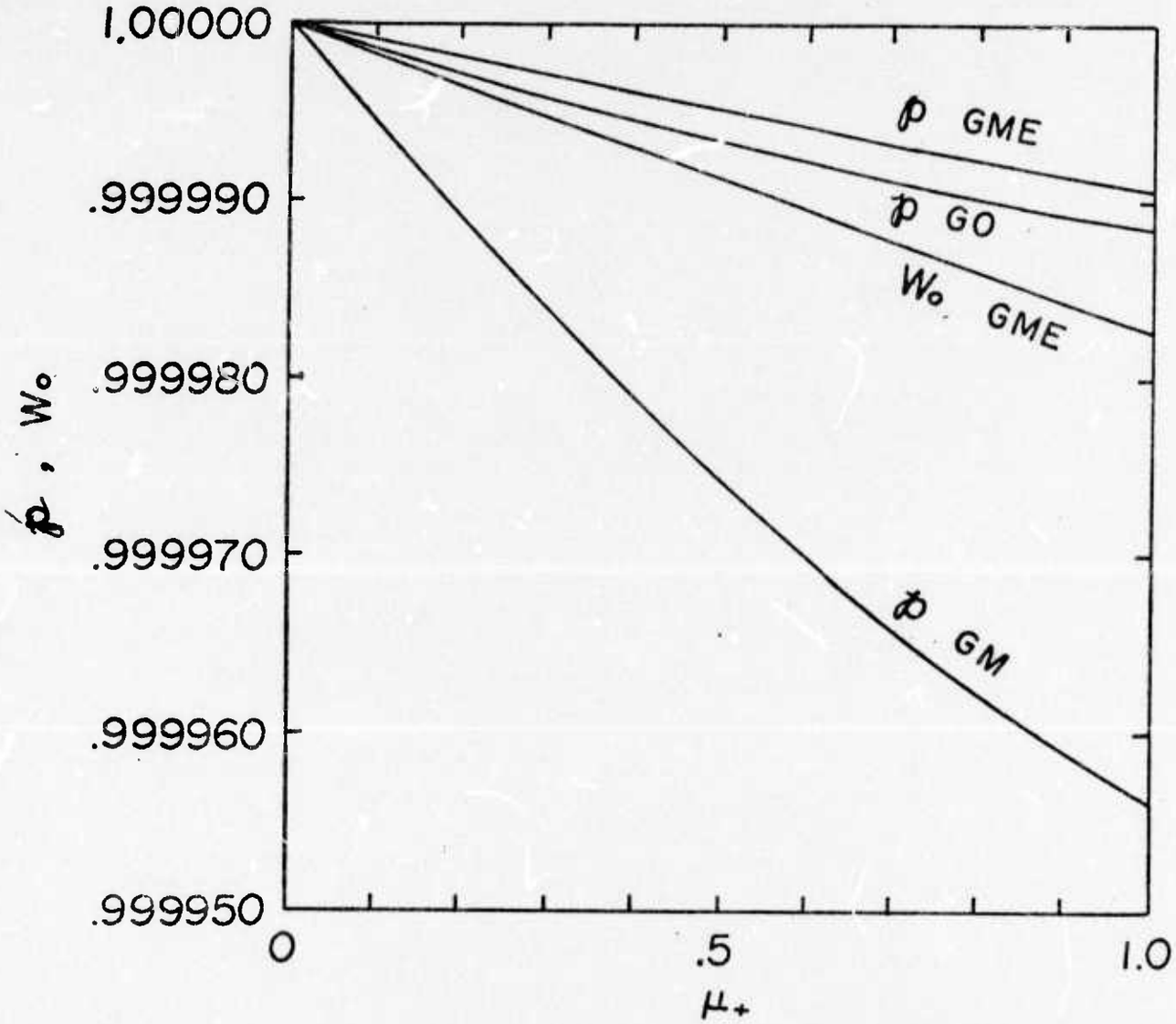
1.00000
.999990
.999980
.999970
.999960
.999950
0
.5
1.0
μ_+
ϕ, W_0
ϕ GME
ϕ GO
W_0 GME
ϕ GM

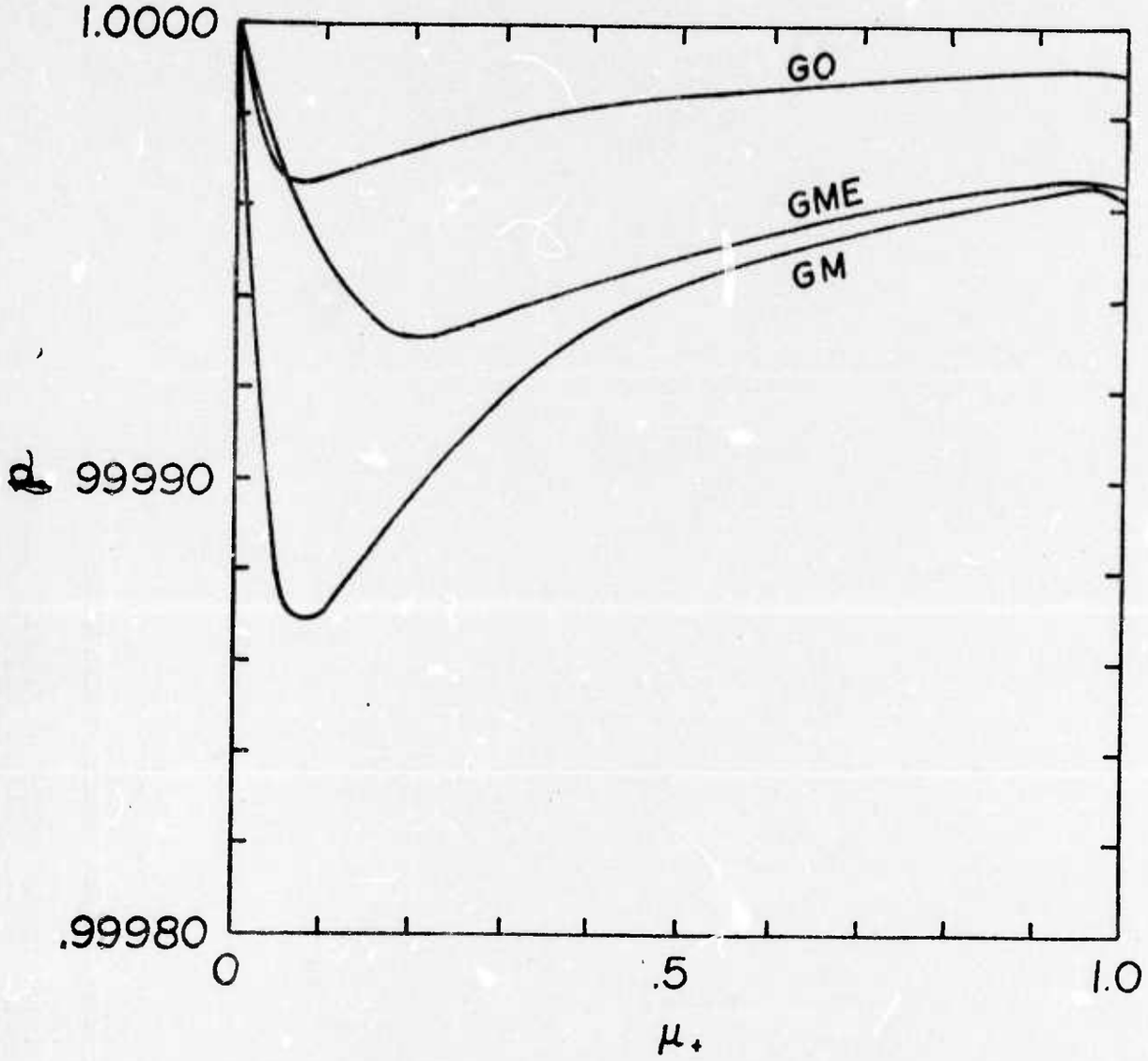
1.0000
GO
GME
GM
99990
.99980
0
.5
1.0
μ.

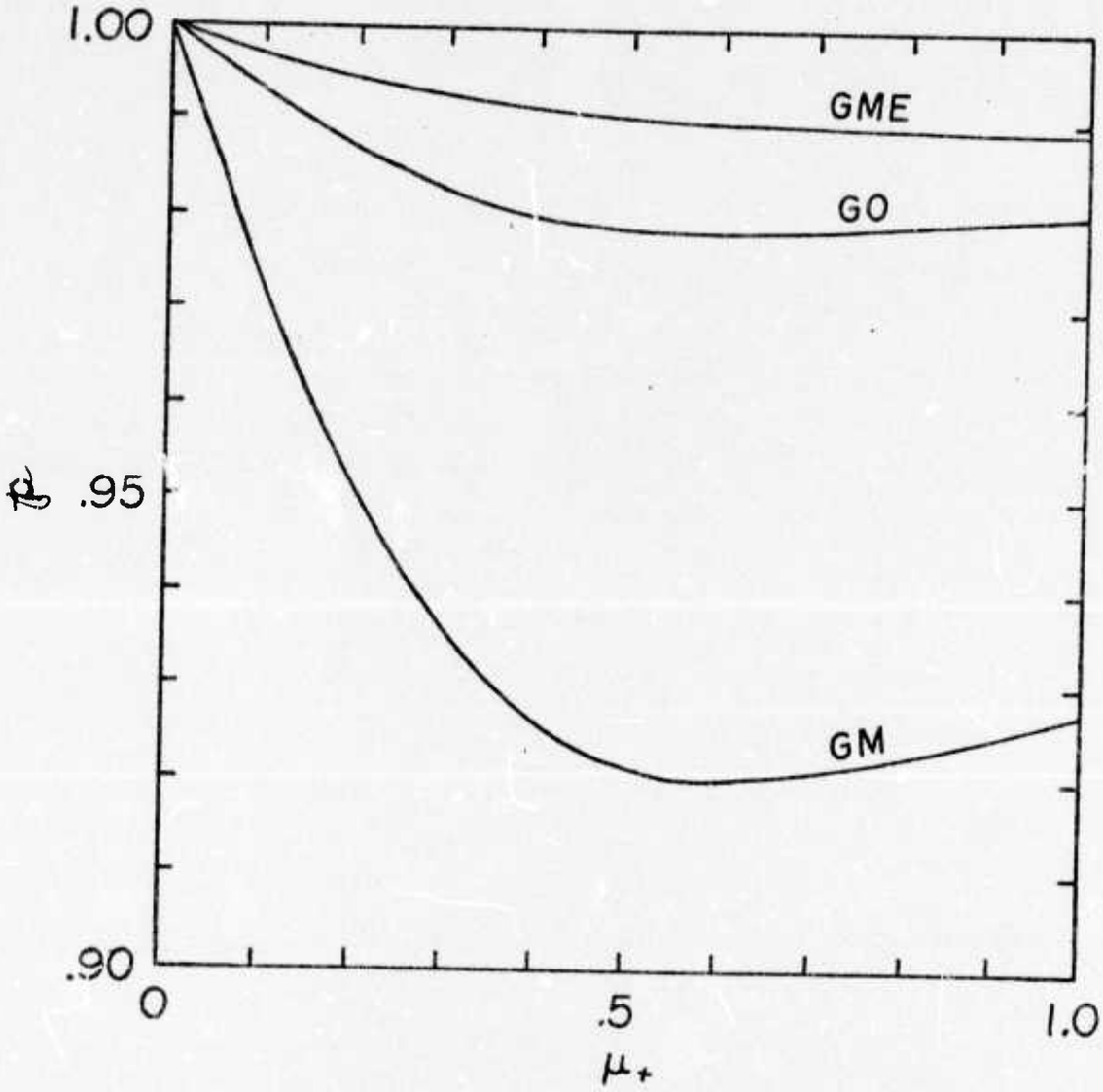
1.00
.95
.90
0
.5
1.0
μ_+
GME
GO
GM

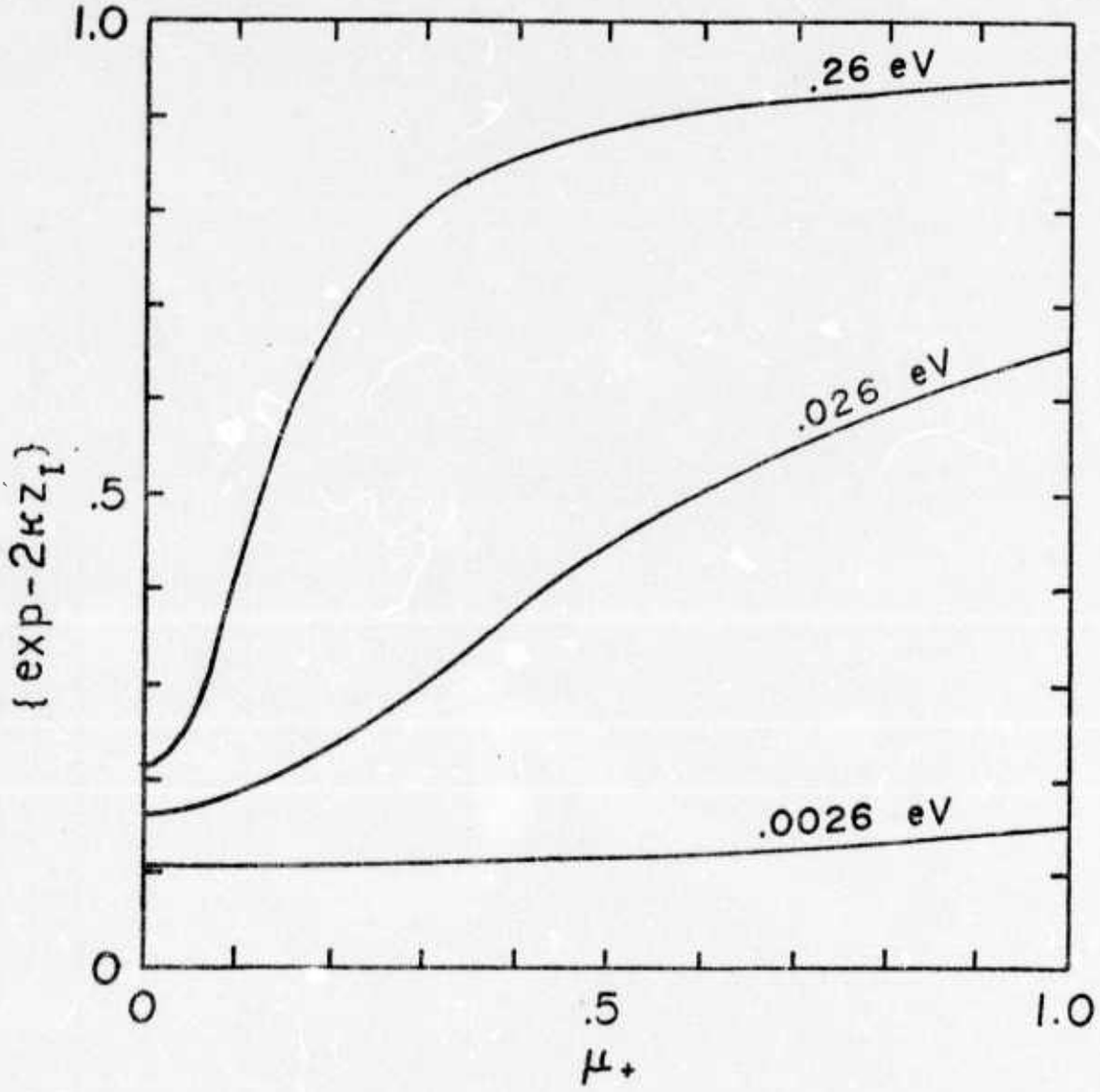

ENCLOSURE (1)

The Connection Between the Thermodynamics of Chemisorption on Semiconductor Surfaces and Surface Scattering of Carriers

Richard F. Greene*
Naval Ordnance Laboratory
White Oak, Maryland 20910

ABSTRACT

An explicit theoretical relation is derived which connects the thermodynamics of chemisorption on semiconductor surfaces with the scattering rate of conduction and valence band carriers by charges localized in the chemisorption bonds.

Enclosure (2)
(reference 17)

I. INTRODUCTION

In surface science it is desirable to make connections between "exterior phenomena", such as chemisorption, and "interior phenomena", such as transport in the semiconductor space charge layer. Of course, it is well known that chemisorption bonds are often charged, producing surface space charge layers of appreciable conductance,[1,2] and it is now also accepted that chemisorption bond charges are strong scatterers of these carriers.[3] In this paper we derive an explicit theoretical relation[4] which ties together chemisorption thermodynamics and surface scattering rates.

We have recently calculated[5] the differential surface scattering rate w, caused by an arbitrary array of surface point charges, for carriers in a semiconductor. We expressed w in terms of the statistical structure factor $S(\underset{\sim}{Q})$ of the surface charge array, using the surface response function[6] which gives the scattering potential of the array as a result of screening, dielectric, and image effects. We show, on the basis of statistical thermodynamic ensemble theory, that $S(\underset{\sim}{Q})$ also determines the chemical potential g of the absorbed species. This dual role of $S(\underset{\sim}{Q})$ enables us to derive a new and general relation between surface scattering rates and the adsorption isotherm. Transport measurements may thereby be used to clarify chemisorption processes and vice versa.

II. STATISTICAL STRUCTURE FACTOR OF CHEMISORBED ATOMS

Chemisorbed atoms make their presence felt in carrier scattering through their charge, of course, but also through their arrangement, since that determines electron wave interference effects. For scattering purposes the adion arrangement is best expressed by the statistical structure factor $S(\underset{\sim}{Q})$, which we will develop below. Having done so, we will then show that $S(\underset{\sim}{Q})$ can be expressed in thermodynamic terms, e.g. the chemical potential of the chemisorbed species, at least in the case where the chemisorption has reached equilibrium.

An array of point charges e on a surface corresponds to a surface charge density $\Omega(\underset{\sim}{R})$:

$$\Omega(\underset{\sim}{R}) = e \sum_{\underset{\sim}{R}_i} \delta(\underset{\sim}{R} - \underset{\sim}{R}_i) \tag{1}$$

which has the spatial average

$$\bar{\Omega} = \lim_{L\to\infty} L^{-2} \int d\underset{\sim}{R}\ \Omega_L(\underset{\sim}{R}) \tag{2}$$

($\Omega_L(\underset{\sim}{R})$ is obtained by truncating $\Omega(\underset{\sim}{R})$ to zero outside a macroscopic area L^2.) We use the autocorrelation functions of Ω and $\delta\Omega = \Omega - \bar{\Omega}$:

$$\overline{\Omega(\underset{\sim}{R})\ \Omega(\underset{\sim}{R}+\Delta\underset{\sim}{R})} = \lim_{L\to\infty} L^{-2} \int_{L^2} d\underset{\sim}{R}\ \Omega_L(\underset{\sim}{R})\ \Omega_L(\underset{\sim}{R}+\Delta\underset{\sim}{R}). \tag{3a}$$

$$\overline{\delta\Omega(\underset{\sim}{R})\ \delta\Omega(\underset{\sim}{R}+\Delta\underset{\sim}{R})} = \overline{\Omega(R)\ \Omega(R+\Delta R)} - \bar{\Omega}^2 \quad . \tag{3b}$$

[illegible] (2)

In scattering theory it is convenient to work with the Fourier transforms

$$\Omega(\underset{\sim}{Q}) = (2\pi)^{-1} \int d\underset{\sim}{R}\ \Omega(\underset{\sim}{R})\ e^{-i\underset{\sim}{Q}\cdot\underset{\sim}{R}} \tag{4a}$$

$$\delta\Omega(\underset{\sim}{Q}) = (2\pi)^{-1} \int d\underset{\sim}{R}\ \delta\Omega(\underset{\sim}{R})\ e^{-i\underset{\sim}{Q}\cdot\underset{\sim}{R}}$$

$$= \Omega(\underset{\sim}{Q}) - 2\pi\bar{\Omega}\delta(\underset{\sim}{Q}) \quad \text{etc.} \tag{4b}$$

Using the truncated functions $\Omega_L(R)$, etc. one can form the spectral density[6]

$$\mathcal{J}_{\Omega}(\underset{\sim}{Q}) = \lim_{L\to\infty} L^{-2}|\Omega_L(\underset{\sim}{Q})|^2 \tag{5}$$

which has the transform (Wiener-Khintchine formula[7])

$$\mathcal{J}_{\Omega}(\underset{\sim}{Q}) = (4\pi^2)^{-1} \int d\Delta\underset{\sim}{R}\ \overline{\Omega(\underset{\sim}{R})\ \Omega(\underset{\sim}{R}+\Delta\underset{\sim}{R})}\ e^{-i\underset{\sim}{Q}\cdot\Delta\underset{\sim}{R}}. \tag{6}$$

Likewise, the spectral density of $\delta\Omega$ is

$$\mathcal{J}_{\delta\Omega}(\underset{\sim}{Q}) = (2\pi)^{-2} \int d\Delta\underset{\sim}{R}\ (\Omega(\underset{\sim}{R})\ \Omega(\underset{\sim}{R}+\Delta\underset{\sim}{R}) - \bar{\Omega}^2)\ e^{-i\underset{\sim}{Q}\cdot\Delta\underset{\sim}{R}}$$

$$= \mathcal{J}_{\Omega}(\underset{\sim}{Q}) - \bar{\Omega}^2\delta(\underset{\sim}{Q}) \quad . \tag{7}$$

We confine our attention to chemisorption charges e which lie at lattice points $\underset{\sim}{A}$ which have some definite relation to the 3-dimensional crystal lattice. Then Eq. (1) can be written

$$\Omega(\underset{\sim}{R}) = e \sum_{\underset{\sim}{A}} n(\underset{\sim}{A})\delta(\underset{\sim}{R} - \underset{\sim}{A}); \quad (n(\underset{\sim}{A}) = 0,\ 1 \text{ only},) \tag{8}$$

where $n(\underset{\sim}{A})$ is the occupation number for surface lattice site $\underset{\sim}{A}$. Of course,

$$\bar{\Omega} = e\,\bar{n}/a_o \quad , \tag{9}$$

(2)

where $\bar{n}$ is the mean occupation number, and a_o is the unit cell area of the surface lattice. Using Eqs. (6) and (8) one can write

$$\mathcal{J}_\Omega(Q) = (e^2/4\pi^2) \lim_{L\to\infty} L^{-2} \sum_{\underset{\sim}{A}}^{(L)} \sum_{\underset{\sim}{A}'}^{(L)} m(\underset{\sim}{A}) n(\underset{\sim}{A}') \, e^{i\underset{\sim}{Q}\cdot(\underset{\sim}{A}-\underset{\sim}{A}')}, \tag{10}$$

where the sum goes over the points $\underset{\sim}{A}$ and $\underset{\sim}{A}'$ within the area L^2.

It is sufficient to consider only those ensembles which have spatial uniformity, in the sense that (denoting ensemble averages $\{\}$)

$$\{n(\underset{\sim}{A}) n(\underset{\sim}{A}+\Delta\underset{\sim}{A})\} = \bar{n}\, p(\Delta\underset{\sim}{A}), \quad \text{independent of } \underset{\sim}{A}. \tag{11}$$

$p(\Delta\underset{\sim}{A})$ is then the conditional occupation number of site $\underset{\sim}{A}+\Delta\underset{\sim}{A}$ when $n(\underset{\sim}{A}) = 1$, and $p(0) \equiv 1$. When Eq. (11) is ensemble averaged, the $\sum_{\underset{\sim}{A}}$ summation becomes trivial and one gets:

$$\{\mathcal{J}_\Omega(Q)\} = (ne^2/4\pi^2 a_o) \sum_{\Delta\underset{\sim}{A}} p(\Delta\underset{\sim}{A}) \, e^{-i\underset{\sim}{Q}\cdot\Delta\underset{\sim}{A}} \tag{12a}$$

$$= (\bar{n}e^2/4\pi^2 a_o) \sum_{\Delta\underset{\sim}{A}} (p(\Delta\underset{\sim}{A}) - \bar{n}) e^{-i\underset{\sim}{Q}\cdot\Delta\underset{\sim}{A}} + \bar{\Omega}^2 \sum_{\hat{\underset{\sim}{Q}}} \delta(\underset{\sim}{Q}-\hat{\underset{\sim}{Q}}), \tag{12b}$$

where the $\hat{\underset{\sim}{Q}}$ are all the reciprocal lattice vectors

$$\hat{\underset{\sim}{Q}}\cdot\underset{\sim}{A} = 2\pi \text{ integer or zero.} \tag{12c}$$

and we used the identity

$$\sum_{\Delta\underset{\sim}{A}} e^{i\underset{\sim}{Q}\cdot\Delta\underset{\sim}{A}} = (4\pi^2/a_o) \sum_{\hat{\underset{\sim}{Q}}} (\underset{\sim}{Q} - \hat{\underset{\sim}{Q}}) \tag{12d}$$

Instead of the periodic function $\{\mathcal{J}_\Omega(Q)\}$, it proves more convenient in scattering theory to use the non-periodic spectral density of $\delta\Omega = \Omega - \bar{\Omega}$. From Eq. (7) one gets

ENCLOSURE (2)

$$\{\mathscr{I}_{\delta\Omega}(Q)\} = (a_o\, \bar{\Omega}^2/4\pi^2)\, S(\underset{\sim}{Q}) \ , \qquad (13a)$$

where $S(\underset{\sim}{Q})$ is the statistical structure factor:

$$S(\underset{\sim}{Q}) = \sum_{\Delta\underset{\sim}{A}} ((p(\Delta\underset{\sim}{A})/\bar{n} - 1))\, e^{-i\underset{\sim}{Q}\cdot\Delta\underset{\sim}{A}} + (4\pi^2/a_o) \sum_{\hat{\underset{\sim}{Q}}\neq 0} \delta(\underset{\sim}{Q}-\hat{\underset{\sim}{Q}}). \qquad (13b)$$

The statistical structure factor $S(\underset{\sim}{Q})$ shows "Bragg peaks" $\underset{\sim}{Q}=\hat{\underset{\sim}{Q}}$ which correspond to complete order, $\bar{n} = 1$. When $n \neq 1$, there is generally also a continuous "background" which is determined by the pair correlation function $p(\Delta\underset{\sim}{A})$, i.e. the degree of order.

Having expressed the adion arrangement in terms of the statistical structure factor, the form most suitable[5] for calculation of carrier scattering, we want to bring out a different aspect of $S(\underset{\sim}{Q})$. We will show, in fact, that $S(\underset{\sim}{Q})$ can be expressed, by the methods of statistical thermodynamics, in terms of thermodynamic properties chemisorbing species, e.g. the chemical potential g. To do this we have to fill out the description of the system a little: we let the system consist of chemisorbed atoms, of a particular species, on a crystal face. The system is in thermodynamic equilibrium with a reservoir of that species with temperature T and chemical potential g. The grand canonical ensemble is then appropriate and gives the exact result[8]

$$\bar{n}S(0) = \sum_{\Delta\underset{\sim}{A}} (p(\Delta\underset{\sim}{A}) - \bar{n}) = (\{N^2\}-\{N\}^2)/\, N \qquad (14)$$

where N is the fluctuating total number of atoms chemisorbed on a macroscopic crystal surface. The virtue of Eq. (14) is that the R.H.S. is an equilibrium extensive parameter fluctuation which can be expressed exactly[9] in terms of the

(9)

corresponding free energy properties:

$$\{N^2\} - \{N\}^2 = kT\, \partial\{N\}/\partial g)_T \quad . \quad g = \text{chemical potential} \tag{15}$$

(The unit cell dimension a_o is considered as a fixed extensive parameter.) Thus one obtains the basic thermodynamic property of the statistical structure factor.

$$\{S(0)\} = (kT/\bar{n}^2)\partial\bar{n}/\partial g)_{T,A_o} \tag{16}$$

Some insight into Eq. (16) is provided by the simplest adsorption model, in which interaction between adsorbed molecules is ignored. The system energy and grand partition function are then

$$E = \sum_{\underset{\sim}{A}} n(\underset{\sim}{A})\varepsilon(\underset{\sim}{A}) = \varepsilon_o N \; ; \quad n(\underset{\sim}{A}) = 0, 1 \tag{17a}$$

$$Q = \sum_{\underset{\sim}{n}} \exp\left((\varepsilon_o - g)\, N/kT\right) \tag{17b}$$

Because of the formal similarity of this model to that of the non-interacting Fermi gas one can immediately write down

$$\bar{n} = [1 + \exp((\varepsilon_o - g)/kT)2]^{-1}. \tag{18}$$

This can be seen[10] to be the familiar Langmuir isotherm[11] if we assume that the gas, with which the adsorbed species is in equilibrium, is at moderate temperature T and pressure p: Then the ideal gas relation

$$e^{-g/kT} = (2\pi mkT/h^2)^{3/2}\,(kT/p) \tag{19}$$

can be used. This isotherm satisfies the relation

$$\frac{kT}{\bar{n}^2}\frac{\partial\bar{n}}{\partial g}\bigg|_T = 1/n - 1 \quad \text{(Random case)} \tag{20}$$

(2)

On the other hand, the lack of interaction between adatoms means we can assume zero positional autocorrelation: $p(\Delta\underset{\sim}{A}) = \bar{n}$ for $\Delta\underset{\sim}{A} \neq 0$. Then Eq. (13b) tells us that

$$S(0) = 1/\bar{n} - 1 \quad \text{(Random case)} \tag{21}$$

Thus Eq. (16) is satisfied for this simplest model, independent of the general thermodynamic fluctuation argument.

It is important to note that Eq. (20) breaks down even for the simplest model involving Coulomb or other interactions. The system energy can be written as

$$E = \sum_{A} n(\underset{\sim}{A})(\varepsilon_o + 1/2\ e\phi(\underset{\sim}{A})); \qquad n(A) = 0,1 \tag{22}$$

where $\phi(\underset{\sim}{A})$ is the potential at $\underset{\sim}{A}$ due to the other adions, screening, and polarization, and hence depends on the entire set of occupation numbers $n(\underset{\sim}{A})$. We make the drastic approximation of replacing $\phi(\underset{\sim}{A})$ by ϕ_{ps}, the surface potential in the planar semiconductor band-bending model of Kingston and Neustadter[12] in which ϕ_{ps} is determined entirely by $\bar{n}$, T, and material constants. The grand partition function then reduces to Eq: (17b), except that g is replaced by $g - 1/2e\phi_{ps}(\bar{n})$. We can therefore immediately write down the "band-bending isotherm"

$$\bar{n} = [1 + \exp((\varepsilon_o - g + 1/2e\phi_{ps}(\bar{n}))/kT]^{-1} \tag{23}$$

in which the coverage $\bar{n}$ is smaller than in the Langmuir isotherm. Eq. (20) is now replaced by

$$\frac{kT}{\bar{n}^2}\left.\frac{\partial \bar{n}}{\partial g}\right|_T = (1/n - 1)/(1 + 1/2\ \bar{n}^2\ \partial u_{ps}/\partial \bar{n}\ _T) \qquad (24)$$

where $u_{ps} = e\phi_{ps}/kT$. We cannot, however, conclude anything about $p(\Delta\underset{\sim}{A})$ from such a sketchy treatment except, of course, that Eq. (16) must be satisfied because of the general equilibrium fluctuation arguments.

III. SURFACE SCATTERING-CHEMICAL POTENTIAL RELATION

Recently a calculation[5] has been made of the surface scattering of conduction electrons by a partially correlated array of surface point charges, or, more precisely, by the screened potential of this array. The differential scattering probability w for the process $|\underset{\sim}{K},k_z> \rightarrow |\underset{\sim}{K}+\underset{\sim}{Q},k_z'>$ (where $\underset{\sim}{K}$ is the surface component of the wave vector, and $\underset{\sim}{K}^2 + k_z^2 = k_z'^2 + (\underset{\sim}{K} + \underset{\sim}{Q})^2$) was found, in the Born approximation, to have the form

$$w(\mu,\eta) = w(\mu,\eta)_{GO}\, B(\exp - 2\kappa Z_I)\, S(\underset{\sim}{Q} - \underset{\sim}{K}) \qquad (25)$$

Here w_{GO} is the scattering rate for a random array of Yukawa potentials on the surface, B is the surface space charge form factor which corrects for the actual form of the space charge potential, and $(\exp - 2\kappa Z_I)$ is a correction factor for the dielectric image potential. We emphasize that all the information about the actual distribution of the scattering centers over the surface is contained in S, and the rest of the expression need be calculated only once and applies to any surface distribution.

Frequently in the chemisorption of ionizing atoms on semiconductors the autocorrelation $p(\Delta\underset{\sim}{A})$ has a short range compared to the electron wavelength:

$$p(\Delta\underset{\sim}{A}) = \bar{n} \text{ for all } |\Delta\underset{\sim}{A}|\, k_o \gtrsim 1. \qquad (26)$$

In that case we immediately get that

$$S(\underset{\sim}{Q} - \underset{\sim}{K}) = S(0) \qquad (27)$$

(2)

for all values of $\underset{\sim}{Q} - \underset{\sim}{K}$ appearing in Eq. (25). One then has, using Eq. (16),

$$w(\mu,\eta) = w(\mu,\eta)_{\text{random}} \; (kT/\bar{n}(1-\bar{n}))(\partial\bar{n}/\partial g)_T \qquad (28)$$

which is the fundamental relation between surface scattering rate and chemical potential of the scatterer.

We may now make a direct and useful connection with surface transport theory, e.g. with the semiconductor field effect or the size effect of thin films. Here the surface scattering rates enter the theory through the Fuchs reflectivity p, according to the recipe[13]

$$p(\mu) = 1 - \int_{-1}^{0} d\mu_- \int_0^2 d\Delta\eta(-\mu/\mu_-)w(\mu_-,\eta)\left\{1 - \cos\sqrt{\frac{1-\mu_-^2}{1-\mu^2}}\right\} \qquad (29)$$

Since S(0) is independent of angle, we immediately obtain an analog of Eq. (28) for the Fuchs reflectivity:

$$p(\mu) = p(\mu)_{\text{random}} \; (kT/\bar{n}(1-\bar{n}))(\partial\bar{n}/\partial g)_T \qquad (30)$$

Now p_{random} can be calculated[5] once and for all for a given surface: it does not depend upon the actual distribution of the adions, but only on their total number. For any actual chemisorption equilibrium, departures from the Langmuir isotherm will be produced by adion-adion interactions, as noted in the discussion of Eqs. (20) and (24). These departures can be measured, e.g., by simultaneous measurements of pressure and Hall coefficient, the latter providing a means[14] of inferring the coverage $\bar{n}$. The Fuchs reflectivity can be

2

inferred from surface mobility measurements. To test Eq. (30) it would thus seem necessary to make simultaneous measurements of pressure, coverage, and galvanomagnetic response on a single-crystal semiconductor face which is otherwide clean to ultrahigh vacuum standards. Such measurements, involving various gases on epitaxial IV-VI semiconductor faces, are being carried out at the Naval Ordnance Laboratory by R. N. Lee.[15] Although the present treatment is restricted to monolayer adsorption with only short range order, it is hoped that Eq. (30) will provide a means of applying observations of transport inside a semiconductor to measurements of chemisorption on the outside, and vice versa.

IV. ACKNOWLEDGMENTS

The author is grateful to Drs. J. R. Cullen and R. N. Lee for valuable and stimulating comments on many aspects of this work. Thanks for helpful discussions are also due to Drs. G. Belton, N. Gjostein, G. Hudson, B. V. Kessler, F. Stern, and J. N. Zemel

(2)

APPENDIX A

The analog of Eq. (16) in the theory of liquids is derived[8] in ensemble theory by approximating the sum over states by a classical integral over 3N particle coordinates and momenta, corrected by a factor $(n!h^{3N})^{-1}$ to account for indistinguishability and the uncertainty principle. We show below that Eq. (16) is exact for a lattice gas, by using the occupation number description, which is a proper generic phase description. The result is slightly different from the classical continuum case.

From the general weight functions $P_N(\underset{\sim}{n})$ and $P(N,\underset{\sim}{n})$, for the canonical and the grand canonical ensemble, resp., we want to get the two-site joint occupation probabilities $P_N^{(2)}(n(\underset{\sim}{A}_1), n(\underset{\sim}{A}_2))$ and $P^{(2)}(n(\underset{\sim}{A}_1), n(\underset{\sim}{A}_2))$. (subscript N indicates the constraint $\sum_{\underset{\sim}{A}} n(\underset{\sim}{A}) = N$ = fixed, and $\underset{\sim}{n}$ stands for a "value" of the set of all occupation numbers $n(A)$). One has

$$P_N^{(2)}(n(\underset{\sim}{A}_1), n(\underset{\sim}{A}_2)) = \sum_{\underset{\sim}{n}}{}''' P_N(\underset{\sim}{n}) , \tag{A1}$$

where the summation $\sum_{\underset{\sim}{n}}{}'''$ is subject to three constraints:

$n(\underset{\sim}{A}_1)$ = fixed, $n(\underset{\sim}{A}_2)$ = fixed, and $\sum_{\underset{\sim}{A}} n(\underset{\sim}{A}) = N$ = fixed. Then, summing over all values of $n(\underset{\sim}{A}_1)$ and $n(\underset{\sim}{A}_2)$, one gets

$$\sum_{n(\underset{\sim}{A}_1)} \sum_{n(\underset{\sim}{A}_2)} n(\underset{\sim}{A}_1)n(\underset{\sim}{A}_2)P_N^{(2)}(n(\underset{\sim}{A}_1),n(\underset{\sim}{A}_2)) = \sum_{\underset{\sim}{n}}{}' n(\underset{\sim}{A}_1)n(\underset{\sim}{A}_2) P_N(\underset{\sim}{n}), \tag{A2}$$

where $\sum_{\underset{\sim}{n}}{}'$ is subject only to the constraint $\sum_{\underset{\sim}{A}} n(\underset{\sim}{A}) = N$ = fixed.

Since $n(\underset{\sim}{A}) = 0$ or 1 only, Eq. (A2) reduces to

(2)

$$P_N^{(2)}(n(\underset{\sim}{A}_1) = 1,\ n(\underset{\sim}{A}_2) = 1) = \sum_{\underset{\rightarrow}{n}} n(\underset{\sim}{A}_1)\ n(\underset{\sim}{A}_2)\ P_N(\underset{\rightarrow}{n}) \quad . \tag{A3}$$

Next, we sum over all pairs of sites $A_1 \neq A_2$, getting

$$\sum_{\underset{\sim}{A}_1 \neq \underset{\sim}{A}_2} \sum P_N^{(2)}(n(\underset{\sim}{A}_1) = 1,\ n(\underset{\sim}{A}_2) = 1) = \sum_{\underset{\rightarrow}{n}} \sum_{\underset{\sim}{A}_1 \neq \underset{\sim}{A}_2} n(\underset{\sim}{A}_1)n(\underset{\sim}{A}_2)\ P_N(\underset{\rightarrow}{n})$$

$$= N(N-1) \sum_{\underset{\rightarrow}{n}} P_N(\underset{\rightarrow}{n}) = N(N-1) \tag{A4}$$

This procedure can be repeated for the grand canonical ensemble, using the easily obtained identity.

$$P^{(2)}(n(\underset{\sim}{A}_1) = 1, n(\underset{\sim}{A}_2) = 1) = \sum_N P(N)\ P_N^{(2)}(n(\underset{\sim}{A}_1) = 1,\ n(\underset{\sim}{A}_2) = 1), \tag{A5}$$

where P(N) is the probability, in the grand canonical ensemble, that there are exactly N particles in the system. Summing, again, over all pairs of sites $\underset{\sim}{A}_1 \neq \underset{\sim}{A}_2$, one obtains from Eq. (A4) that

$$\sum_{\underset{\sim}{A}_1 \neq \underset{\sim}{A}_2} \sum P^{(2)}(n(\underset{\sim}{A}_1) = 1,\ n(\underset{\sim}{A}_2) = 1) = \sum_N P(N)\ N(N-1) = \{N^2\} - \{N\}. \tag{A6}$$

But, making the identification

$$P^{(2)}(n(\underset{\sim}{A}_1) = 1,\ n(\underset{\sim}{A}_2) = 1) = \{n(\underset{\sim}{A}_1)n(\underset{\sim}{A}_2)\} = \bar{n}\ p(\underset{\sim}{A}_2 - \underset{\sim}{A}_2), \tag{A7}$$

where in the last step we again assumed spatial uniformity in the ensemble, Eq. (A6) gives

$$\{N\} \sum_{\Delta\underset{\sim}{A}} p(\Delta\underset{\sim}{A}) = \{N^2\} - \{N\}, \tag{A8}$$

because $\{N\}/n$ is the total number of sites. We thus get

$$\{N\} \sum_{\Delta\underset{\sim}{A}} p(\Delta\underset{\sim}{A}) = \{N^2\} \tag{A9a}$$

$$\text{or } \{N\} \sum_{\Delta\underset{\sim}{A}} (p(\Delta\underset{\sim}{A}) - \bar{n}) = \{N^2\} - \{N\}^2 \tag{A9b}$$

$$\text{or } \{N\} \sum_{\Delta\underset{\sim}{A}\neq 0} (p(\Delta\underset{\sim}{A}) - \bar{n}) = \{N^2\} - \{N\}^2 (1-\bar{n}). \tag{A9c}$$

In the classical treatment $(1-\bar{n})$ is replaced by unity.[8]

(2)

REFERENCES

*Supported by Advanced Research Projects Agency, Department of Defense

+Two dimensional vectors are written in bold face capitals.

1. A. Many, Y. Goldstein, and N. B. Grover, "Semiconductor Surfaces" North Holland Publishing Co. (Amsterdam, 1965).
2. K. Hauffe and Th. Wolkenstein, editors, "Electronic Phenomena in Chemisorption and Catalysis on Semiconductors" Walter deGruyter & Co. (Berlin, 1969).
3. M. Greene, editor, "Solid State Surface Science, Vol. I" Marcel Dekker (New York, 1969) Chapter 2.
4. A preliminary form of this relation was reported by the author at the 1972 Thin Film Conference (Venice, Italy, 18 May 1972) and at the 1972 Surface Science Conference (Rolla, Missouri, 14 July 1972).
5. R. F. Greene and J. Malamas, to be published, Phys. Rev. B2.
6. R. F. Greene, D. Bixler, and R. N. Lee, J. Vac. Sci. and Tech. 8, 75 (1971), to be published.
7. Ming Chen Wang and G. E. Uhlenbeck, Rev. Mod. Phys. 17, 323 (1945).
8. S. A. Rice and P. Gray, "The Statistical Mechanics of Simple Liquids," Interscience (New York, 1965).
9. R. F. Greene and H. B. Callen, Phys. Rev. 83, 1231 (1951).
10. S. C. Kar, Physikal. Zeits. 26, 615 (1925)
    R. H. Fowler and E. A. Guggenheim, "Statistical Thermodynamics" Cambridge University Press, 1949, page 426 et seq.

11. I. Languir, J. Am. Chem. Soc. 40, 1361 (1918).

12. R. H. Kingston and S. F. Neustadter, J. Appl. Phys. 26, 718 (1955), C. G. B. Garrett and W. H. Brattain, Phys. Rev. 99, 376 (1955), R. Seiwatz and M. Green, J. Appl. Phys. 29, 1034 (1958).

13. R. F. Greene, Phys. Rev. 141, 687 (1966).

14. M. H. Brodsky and J. N. Zemel, Phys. Rev. 155, 780 (1967) G. F. McLane and J. N. Zemel, Thin Solid Films 7, 229 (1971) R. F. Egerton and A. J. Crocker, Surface Science 27, 117 (1971).

15. R. N. Lee, private communication (1972).